NASA/TM—2020–219744

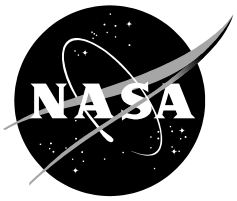

Improved Methods for Hyperelastic Material Characterizations Based on Uniaxial, Radial-Biaxial, and Strip-Biaxial Test Data

William L. Ko, Claudia Herrera, Ray Sadler, and David Neufeld
NASA Armstrong Flight Research Center, Edwards, California

Shun-Fat Lung
Jacobs Technology, Inc., Edwards, California

May 2019

NASA STI Program ... in Profile

Since its founding, NASA has been dedicated to the advancement of aeronautics and space science. The NASA scientific and technical information (STI) program plays a key part in helping NASA maintain this important role.

The NASA STI program operates under the auspices of the Agency Chief Information Officer. It collects, organizes, provides for archiving, and disseminates NASA's STI. The NASA STI program provides access to the NTRS Registered and its public interface, the NASA Technical Reports Server, thus providing one of the largest collections of aeronautical and space science STI in the world. Results are published in both non-NASA channels and by NASA in the NASA STI Report Series, which includes the following report types:

- TECHNICAL PUBLICATION. Reports of completed research or a major significant phase of research that present the results of NASA Programs and include extensive data or theoretical analysis. Includes compilations of significant scientific and technical data and information deemed to be of continuing reference value. NASA counterpart of peer-reviewed formal professional papers but has less stringent limitations on manuscript length and extent of graphic presentations.

- TECHNICAL MEMORANDUM. Scientific and technical findings that are preliminary or of specialized interest, e.g., quick release reports, working papers, and bibliographies that contain minimal annotation. Does not contain extensive analysis.

- CONTRACTOR REPORT. Scientific and technical findings by NASA-sponsored contractors and grantees.

- CONFERENCE PUBLICATION. Collected papers from scientific and technical conferences, symposia, seminars, or other meetings sponsored or co-sponsored by NASA.

- SPECIAL PUBLICATION. Scientific, technical, or historical information from NASA programs, projects, and missions, often concerned with subjects having substantial public interest.

- TECHNICAL TRANSLATION. English-language translations of foreign scientific and technical material pertinent to NASA's mission.

Specialized services also include organizing and publishing research results, distributing specialized research announcements and feeds, providing information desk and personal search support, and enabling data exchange services.

For more information about the NASA STI program, see the following:

- Access the NASA STI program home page at http://www.sti.nasa.gov

- E-mail your question to help@sti.nasa.gov

- Phone the NASA STI Information Desk at 757-864-9658

- Write to:
  NASA STI Information Desk
  Mail Stop 148
  NASA Langley Research Center
  Hampton, VA 23681-2199

NASA/TM—2020–219744

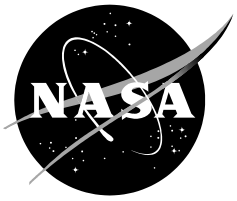

Improved Methods for Hyperelastic Material Characterizations Based on Uniaxial, Radial-Biaxial, and Strip-Biaxial Test Data

William L. Ko, Claudia Herrera, Ray Sadler, and David Neufeld
NASA Armstrong Flight Research Center, Edwards, California

Shun-Fat Lung
Jacobs Technology, Inc., Edwards, California

National Aeronautics and
Space Administration

Armstrong Flight Research Center
Edwards, California 93523-0273

May 2019

Acknowledgments

The authors express their deep appreciation to National Aeronautics and Space Administration (NASA) Space Technology Mission Directorate and Armstrong Flight Research Center (AFRC) Chief Technologist David Voracek for granting the Center Innovation Fund (CIF) for supporting the present research. The authors also express their sincere thanks to CIF original principal investigator Eric Miller for initiating the fundamental research of hyperelastic materials for flight applications, and for technical encouragement and support during the course of this CIF research.

The authors additionally express their sincere thanks to NASA AFRC Flight Loads Laboratory (FLL) technicians Jeffrey Howell, Jacob Roepel, and Aaron Rumsey, who helped with the design and construction of an innovative radial-biaxial test round-table system, and who, with the support of a testing-data-gathering computer system and software maintained by NASA AFRC system administrator Joel Bremer, successfully carried out the experimental program and obtained uniaxial and biaxial stress-stretch data for material characterization of a silicone rubber (a potential candidate hyperelastic material for aerospace applications).

The authors also thank NASA FLL Test Operations Manager Ronnie Haraguchi for testing various specimen-gripping methods for solving the specimen-slipping problems; and paving the way for invention of an end-folding method for uniaxial and strip-biaxial test specimens, and a webbing-looped flexible bonding method for pulling radial-biaxial test specimens, enabling the specimens to reach high extension ratios without premature failures.

Finally, the authors thank NASA summer intern student Louis Edelman for providing experimental data reductions and valuable plots for determinations of material constants for the silicone rubber.

Table of Contents

Abstract

This report concerns the different analytical methods used for material characterizations of hyperelastic silicone rubber, a potential candidate elastomer for aerospace applications. To establish the constitutive equations for the silicon rubber, strain-energy gradients (material constants) must be determined from experiments.

Earlier experiments by Blatz-Ko showed that the material constants of natural rubber determined from different stress fields were different. Therefore, in the current material characterization, uniaxial, equal-biaxial, and strip-biaxial tensile tests were conducted. Based on the resulting stress-stretch data, the material constants were determined by using a trendline on the stress-difference plots and energy plots, and also the MSC-Marc® curve-fitting method. The results confirm that the material constants determined from uniaxial and biaxial stress fields are indeed different. The material constants determined from the equal-biaxial energy plots and from the MSC-Marc® combined-curve-fitting method were found to be extremely close, and can be considered as universal material constants for establishing the constitutive equations for the silicone rubber under any stress field.

The results of this report show that a uniaxially stretched specimen became slightly anisotropic due to crystallization of polymer molecular chains, and that equal-biaxial and strip-biaxial testing must be conducted to fully understand the material properties of hyperelastic materials.

Nomenclature

AFRC	Armstrong Flight Research Center
b	undeformed circular specimen outer radius, in.
$\overline{b}$	deformed circular specimen outer radius (or radius of a circular marking on the radial-biaxial tester round table), in.
C_{10}	$= W_1$, Mooney-Rivlin constant, lb/in^2
C_{01}	$= W_2 / J_3^2$, Mooney-Rivlin constant, lb/in^2
DIC	Digital Image Correlation
E	Young's modulus, lb/in^2
FLL	Flight Loads Laboratory
J_1	$= \lambda_1^2 + \lambda_2^2 + \lambda_3^2$, first invariant of Cauchy-Green deformation tensor
J_2	$= \frac{1}{\lambda_1^2} + \frac{1}{\lambda_2^2} + \frac{1}{\lambda_3^2}$, second invariant of Cauchy-Green deformation tensor
J_3	$\lambda_1\lambda_2\lambda_3 = \frac{\text{Deformed volume}}{\text{Undeformed volumn}}$, third invariant of Cauchy-Green deformation tensor
i, j	=1, 2, 3, indices
k	=1, 2, 3, indices
m, n	indices
NASA	National Aeronautics and Space Administration
NTR	New Technology Reporting
P	applied load, lb
T	radial-biaxial specimen pulling-string tension, lb
t	specimen thickness, in.
UAV	unmanned aerial vehicle
W	strain energy density function, (in-lb)/in^3
W_1	$\equiv \frac{\partial W}{\partial J_1}$, first strain energy gradient (material constant), lb/in^2

W_2 $\equiv \frac{\partial W}{\partial J_2}$, second strain energy gradient (material constant), lb/in^2

ε strain in loading direction, in/in

ε_k strain at strain-sensing station k, in/in

ε_{lat} strain in lateral direction, in/in

ν $\equiv -\frac{\ln \lambda_{lat}}{\ln \lambda} = -\frac{\ln(1+\varepsilon_{lat})}{\ln(1+\varepsilon)} \xrightarrow[\text{deformation}]{\text{Small}} -\frac{\varepsilon_{lat}}{\varepsilon}$, modified Poisson's ratio for large deformations

μ shear modulus at small strain $(\lambda_i \to 1)$, lb/in^2

λ_i extension ratio in i (=1, 2, 3)-direction

λ_j extension ratio in j (=1, 2, 3)-direction

λ extension ratio in loading direction

λ_{lat} extension ratio in load-free lateral directions for uniaxial tension

λ_{th} extension ratio in load-free thickness direction for biaxial tension

σ engineering stress (Biot stress) in reference to undeformed cross section, lb/in^2

σ_i engineering stress (Biot stress) in i-direction, lb/in^2

σ_j engineering stress (Biot stress) in j-dirction, lb/in^2

σ_{uni} uniaxial engineering stress (Biot stress) in reference to undeformed cross section, lb/in^2

σ_{e-bi} equal-biaxial engineering stress (Biot stress) in reference to undeformed cross section, lb/in^2

σ_{s-bi} strip-biaxial engineering stress (Biot stress) in reference to undeformed cross section, lb/in^2

$\bar{\sigma}_i$ $= \frac{\sigma_i \lambda_i}{J_3}$, true stress (Cauchy stress) in i-direction referred to deformed cross section, lb/in^2

Introduction

Hyperelastic (rubber-like) materials have wide applications (for example, automobile tires, rubber hoses, shock absorbers, inflatable unmanned aircraft, hover-craft skirts, seismic isolators, et cetera.). In one of the major aerospace applications, rubber materials are used as load-carrying propellants for solid rocket motors (for example, Space Shuttle booster rockets, and various types of missiles).

To establish the constitutive equations for the silicon rubber, strain-energy gradients (material constants) must be determined from experiments. Because of increasing aerospace applications of hyperelastic (viscoelastic) materials [for example, launching vehicle engine vibration damping, structure flutter suppressions, inflatable wing skins of unmanned aerial vehicle (UAV), transition flaps for noise reduction, et cetera], there is a need to fully understand the fundamental mechanical behavior of hyperelastic materials.

Hyperelastic membrane has no compressive strength. When applied to inflatable aircraft, or transition flaps, the hyperelastic skins are highly stretched for maintaining shapes. Ko and Lung (ref. 1) found that, unlike metallic materials for which the stress concentration factors remain constant with deformations, the hyperelastic stress concentration factors for Mooney material (two material constants) increased monotonically with stretching. Because of this non-classical stress concentration behavior, if a sharp particle impinges on the highly stretched hyperelastic skin, high stress concentration around the pinhole could cause instant tearing failure. A pressurized balloon is a good example of a highly stretched hyperelastic skin. When impinging on a sharp object, the balloon can burst instantly because of a high stress concentration around the impinge-generated pinhole.

Mechanical behavior of hyperelastic materials can be described by using the large deformation theory. The constitutive equations in the theory contain strain energy gradient terms (material constants), which

are determined from experiments. Those material constants are needed in the finite-element modeling of hyperelastic materials. In general practice, material constants determined from uniaxial tensile tests are used for establishing the constitutive equations for hyperelastic materials. This practice could be unsound and must be examined.

In aerospace applications, hyperelastic skins are usually under biaxial stress fields, and using the material constants determined only from a uniaxial stress field becomes questionable.

Earlier experiments by Blatz-Ko (refs. 2, 3) showed that the material constants determined from uniaxial and biaxial tensile tests were different due to different degrees of crystallization of the molecular chains (ref. 4). Thus, there is a need to fully examine the variation of the material constants determined from different stress fields.

This present report shows the different analytical methods used to characterize a silicon rubber material (a potential candidate hyperelastic material for aerospace applications) by determining the material constants from uniaxial, equal-biaxial, and strip-biaxial tensile tests.

Based on the stress-stretch data, the material constants were determined by using stress-difference plots, energy plots, and the MSC-Marc® (MSC Software Corporation, Newport Beach, California) (ref. 5) curve fitting method;, and the consistency of the material constants were examined.

It was found that the material constants determined from uniaxial, equal-biaxial, and strip-biaxial stress fields are indeed different like earlier experiments (refs. 2, 3). However, the material constants determined from the equal-biaxial energy plots and from the MSC-Marc® uniaxial/biaxial combined curve-fitting method were found to be extremely close, and could be considered as the universal material constants for establishing the constitutive equations for describing the stress-stretch behavior of the hyperelastic material (silicone rubber) in any stress field.

Larger-Deformation Constitutive Equations

The constitutive equation formulated by Blatz-Ko (refs. 2, 3) for compressible hyperelastic materials has the following form shown in equation (1):

$$\bar{\sigma}_i J_3 = \sigma_i \lambda_i = 2W_1 \lambda_i^2 - \frac{2W_2}{\lambda_i^2} + J_3 W_3 \ ; \quad (i = 1,2,3) \text{ (not summed)} \tag{1}$$

In equation (1), $\{\bar{\sigma}_i, \sigma_i\}$ are respectively the true stresses (Cauchy stresses) and engineering stresses (Biot stresses) in the $i(=1,2,3)$-direction; λ_i is the extension ratio in the $i(=1,2,3)$ direction; $W_1 \left(\equiv \frac{\partial W}{\partial J_1}\right), W_2 \left(\equiv \frac{\partial W}{\partial J_2}\right), W_3 \left(\equiv \frac{\partial W}{\partial J_3}\right)$ are respectively the first, second, and third strain energy gradients (material constants), where W is the strain energy density function; and $J_1 (= \lambda_1^2 + \lambda_2^2 + \lambda_3^2)$, $J_2 (= 1/\lambda_1^2 + 1/\lambda_2^2 + 1/\lambda_3^2)$, and $J_3 (= \lambda_1 \lambda_2 \lambda_3)$ are respectively the first, second, and third invariants of the Cauchy-Green deformation tensor (refs. 2, 3). For incompressible materials $(J_3 = 1)$, the quantities $\{\sigma_i \lambda_i\}$ in equation (1) represent the true stress.

General Stress-Difference Equation

By taking the difference between the stress expression in *i*- and *j*-directions given by equation (1), one can eliminate the compression term $J_3 W_3$ and obtain the general form of the stress-difference equation as (refs. 2, 3) shown in equation (2):

$$\frac{\sigma_i\lambda_i - \sigma_j\lambda_j}{\lambda_i^2 - \lambda_j^2} = 2W_1 + \frac{2W_2}{\lambda_i^2\lambda_j^2} \quad ; \quad (i,j = 1,2,3) \ (i,j \text{ not summed}) \tag{2}$$

In equation (2), $\{\sigma_i, \sigma_j\}$ are respectively the engineering stresses (Biot stresses) in the $\{i,j\}(=1,2,3)$ directions, and $\{\lambda_i, \lambda_j\}$ are respectively the extension ratios in the $\{i,j\}(=1,2,3)$ directions. The stress-difference equation (2) is applicable to both compressible (for example, foamed rubbers) and incompressible hyperelastic materials. Equation (2) is to be used for graphical determinations of the material constants $\{W_1, W_2\}$ from experiments described in the following section.

Special Forms of Stress-Difference Equations

For graphical determinations of material constants $\{W_1, W_2\}$, uniaxial and biaxial tensile test data can be used. The general stress-difference equations (2) can then be written for uniaxial, equal-biaxial, and strip-biaxial stress fields. For the uniaxial case, there are two different stress-difference equations, one for a uniaxial type-1 plot and another for a uniaxial type-2 plot. For the equal-biaxial case, there are also two different equal-biaxial stress difference equations, one for an equal-biaxial type-1 plot and another for an equal-biaxial type 2 plot. For the strip-biaxial case, there is only one stress difference equation. These equations will be described as follows.

Uniaxial Stress-Difference Equations

For uniaxial tension ($\sigma_1 = \sigma_{uni}, \sigma_2 = \sigma_3 = 0$; $\lambda_1 = \lambda$, $\lambda_2 = \lambda_3 = \lambda_{lat}$), the stress difference equation (2) takes on the following forms:

1. For Uniaxial Type-1 Plots

$$\frac{\sigma_{uni}\lambda}{\lambda^2 - 1/\lambda} = 2W_1 + \frac{2W_2}{\lambda} \tag{3}$$

Equation (3) is for uniaxial Type-1 plotting of $\frac{\sigma_{uni}\lambda}{\lambda^2 - 1/\lambda}$ against $1/\lambda$ for data fitting with a linear trendline to obtain $2W_1$ from the vertical intercept at $1/\lambda = 0$, and obtain $(2W_1 + 2W_2) = \mu$ from the vertical intercept at $1/\lambda = 1$. The value of $2W_2$ can then be calculated from $2W_2 = \underbrace{(2W_1 + 2W_2)}_{\text{Determined}} - \underbrace{2W_1}_{\text{Determined}}$.

2. For Uniaxial Type-2 Plots

If both sides of equation (3) are multiplied by λ, one can obtain an alternative form of uniaxial stress-difference as shown in equation (4):

$$\frac{\sigma_{uni}\lambda^2}{\lambda^2 - 1/\lambda} = 2W_1\lambda + 2W_2 \tag{4}$$

Equation (4) is for uniaxial Type-2 data plotting. Namely, by plotting $\frac{\sigma_{uni}\lambda^2}{\lambda^2-1/\lambda}$ against λ (uniaxial Type-2 data plotting), one can data fit with a linear trendline to obtain $(2W_1+2W_2)=\mu$ from the vertical intercept at $\lambda=1$, and obtain $2W_1$ from the slope of the linear trendline. The value of $2W_2$ can then be calculated from $2W_2=\underbrace{(2W_1+2W_2)}_{\text{Determined}}-\underbrace{2W_1}_{\text{Determined}}$.

3. Limit Values of Uniaxial Type-1 and Type-2 Plots

It is important to mention that in plotting equation (3) or (4), the limit values of $\left(\frac{\sigma_{uni}\lambda}{\lambda^2-1/\lambda}\right)_{\lambda=1}$ [eq. (3)] and $\left(\frac{\sigma_{uni}\lambda^2}{\lambda^2-1/\lambda}\right)_{\lambda=1}$ [eq. (4)] at $\lambda=1$ (that is, $\sigma_{uni}=0$) are neither zero nor indeterminate $(0/0)$, but have a finite value of the shear modulus $\mu[=(2W_1+2W_2)]$ for the incompressible materials $(\nu=0.5)$ as shown below. If $\frac{\sigma_{uni}\lambda}{\lambda^2-1/\lambda}$ and $\frac{\sigma_{uni}\lambda^2}{\lambda^2-1/\lambda}$ are first expanded in the neighborhood of $\lambda\to1$(that is, $\varepsilon\to0$), the limit values of $\left(\frac{\sigma_{uni}\lambda}{\lambda^2-1/\lambda}\right)_{\lambda=1}$ and $\left(\frac{\sigma_{uni}\lambda^2}{\lambda^2-1/\lambda}\right)_{\lambda=1}$ will be the shear modulus μ of the incompressible materials (ν = 0.5).
Based on equation (3), the result is shown in equation (5):

$$\frac{\sigma_{uni}\lambda}{\lambda^2-1/\lambda}\xrightarrow[\varepsilon\to0]{\lambda\to1}\frac{\overbrace{E\varepsilon}^{\sigma_{uni}}(1+\varepsilon)}{(1+\varepsilon)^2-(1+\varepsilon)^{-1}}=\frac{\overbrace{2\mu(1+\nu)}^{E}\varepsilon(1+\varepsilon)}{(1+2\varepsilon+...)-(1-\varepsilon+...)}\xrightarrow[\varepsilon^2\text{neglected}]{\nu=0.5}\frac{3\mu\varepsilon}{3\varepsilon}=\mu \qquad (5)$$

Based on equation (4), the result is shown in equation (6):

$$\frac{\sigma_{uni}\lambda^2}{\lambda^2-1/\lambda}\xrightarrow[\varepsilon\to0]{\lambda\to1}\frac{\overbrace{E\varepsilon}^{\sigma_{uni}}(1+\varepsilon)^2}{(1+\varepsilon)^2-(1+\varepsilon)^{-1}}=\frac{\overbrace{2\mu(1+\nu)}^{E}\varepsilon(1+2\varepsilon+...)}{(1+2\varepsilon+...)-(1-\varepsilon+...)}\xrightarrow[\varepsilon^2\text{neglected}]{\nu=0.5}\frac{3\mu\varepsilon}{3\varepsilon}=\mu \qquad (6)$$

The value $\mu[=(2W_1+2W_2)]$ given by equation (5) or (6) can then be used to confirm the location of the intercept $(2W_1+2W_2)$ of the data-fitting linear trendline at $1/\lambda=1$.

The value of the small-strain shear mosulus $\mu[=E/(1+\nu)=E/3]$ [eq. (3)] can be estimated from the slope of the stress-strain curve at $\lambda\to1$. The estimated value of μ can then be used to indicate the approximate location of the intercept $(2W_1+2W_2)$ of the data-fitting linear trendline at $1/\lambda=1$.

Equal-Biaxial Stress Difference Equations

For the equal-biaxial tension ($\sigma_1=\sigma_2=\sigma_{e-bi}$, , $\sigma_3=0$; $\lambda_1=\lambda_2=\lambda$, $\lambda_3=\lambda_{th}$), the stress difference equation (2) takes on the following forms (refs. 2, 3):

1. For Equal-Biaxial Type-1 Plots

$$\frac{\sigma_{e-bi}\lambda}{\lambda^2-1/\lambda^4}=2W_1+2W_2\lambda^2 \tag{7}$$

Equation (7) is for equal-biaxial Type-1 plotting. Namely, by plotting $\frac{\sigma_{e-bi}\lambda}{\lambda^2-1/\lambda^4}$ against λ^2 and using the data-fitting linear trendline to obtain $(2W_1+2W_2)=\mu$ from the vertical intercept at $\lambda=1$, and obtain $2W_2$ from the slope of the data-fitting linear trendline. Then, $2W_1$ can be calculated from $2W_1=\underbrace{(2W_1+2W_2)}_{\text{Determined}}-\underbrace{2W_2}_{\text{Determined}}$.

2. For Equal-Biaxial Type 2 Plots

Dividing with λ^2, equation (7) can be rewritten in an alternative form as equation (8) for equal-biaxial Type-2 data plotting:

$$\frac{\sigma_{e-bi}\lambda}{\lambda^4-1/\lambda^2}=\frac{2W_1}{\lambda^2}+2W_2 \tag{8}$$

Equation (8) is for equal-biaxial Type-2 plotting. Namely by plotting $\frac{\sigma_{e-bi}\lambda}{\lambda^4-1/\lambda^2}$ against $1/\lambda^2$, and using the data-fitting linear trendline to obtain $2W_2$ from the vertical intercept at $1/\lambda^2=0$, and obtain $(2W_1+2W_2)=\mu$ from the vertical intercept at $1/\lambda^2=1$. Then, $2W_1$ can be obtained from the slope of the data-fitting linear trendline, or can be calculated from $2W_1=\underbrace{(2W_1+2W_2)}_{\text{Determined}}-\underbrace{2W_2}_{\text{Determined}}$.

3. Limit Values of Equal-Biaxial Types-1 and Type-2 Plots

It must be understood that in plotting equation (7) or (8), the reduced plot $\frac{\sigma_{e-bi}\lambda}{\lambda^2-1/\lambda^4}$ against λ^2, or $\frac{\sigma_{e-bi}\lambda}{\lambda^4-1/\lambda^2}$ against $1/\lambda^2$, with the limit value of $\frac{\sigma_{e-bi}\lambda}{\lambda^2-1/\lambda^4}$ or $\frac{\sigma_{e-bi}\lambda}{\lambda^4-1/\lambda^2}$ at $\lambda=1\,(\sigma_{e-bi}\to 0)$ is neither zero nor indeterminate (0/0), but has a finite value of the shear modulus $\mu[=(2W_1+2W_2)]$ for the incompressible materials $(\nu=0.5)$. Namely, if $\frac{\sigma_{e-bi}\lambda}{\lambda^2-1/\lambda^4}$ or $\frac{\sigma_{e-bi}\lambda}{\lambda^4-1/\lambda^2}$ is expanded in the neighborhood of $\lambda\to 1$ (that is, $\varepsilon\to 0$), both of the limit values, $\left(\frac{\sigma_{e-bi}\lambda}{\lambda^2-1/\lambda^4}\right)_{\lambda\to 1}$ or $\left(\frac{\sigma_{e-bi}\lambda}{\lambda^4-1/\lambda^2}\right)_{\lambda\to 1}$, will converge into the shear modulus μ of the incompressible materials (ν = 0.5). Namely, based on equation (7) the result is shown in equation (9):

$$\frac{\sigma_{e-bi}\lambda}{\lambda^2-1/\lambda^4}\xrightarrow[\varepsilon\to 0]{\lambda\to 1}\frac{\overbrace{\left(\frac{E}{1-\nu}\varepsilon\right)}^{\sigma_{e-bi}}(1+\varepsilon)}{(1+\varepsilon)^2-(1+\varepsilon)^{-4}}=\frac{\overbrace{\frac{2\mu(1+\nu)}{1-\nu}}^{E}\varepsilon(1+\varepsilon)}{(1+2\varepsilon+...)-(1-4\varepsilon+...)}\xrightarrow[\varepsilon^2\text{neglected}]{\nu=0.5}\frac{6\mu\varepsilon}{6\varepsilon}=\mu \quad (9)$$

Based on equation (8) the result is shown in equation (10):

$$\frac{\sigma_{e-bi}\lambda}{\lambda^4-1/\lambda^2}\xrightarrow[\varepsilon\to 0]{\lambda\to 1}\frac{\overbrace{\left(\frac{E}{1-\nu}\varepsilon\right)}^{\sigma_{e-bi}}(1+\varepsilon)}{(1+\varepsilon)^4-(1+\varepsilon)^{-2}}=\frac{\overbrace{\frac{2\mu(1+\nu)}{1-\nu}}^{E}\varepsilon(1+\varepsilon)}{(1+4\varepsilon+...)-(1-2\varepsilon+...)}\xrightarrow[\varepsilon^2\text{neglected}]{\nu=0.5}\frac{6\mu\varepsilon}{6\varepsilon}=\mu \quad (10)$$

The value of μ calculated from equations (9) or (10) is finite and is equal to the vertical intercept $(2W_1+2W_2)$ of the data-fitting linear trendline at $\lambda\to 1$.

Strip-Biaxial Stress Difference Equations

For strip-biaxial tension ($\sigma_1=\sigma_{s-bi},\ \sigma_2\neq 0,\ \sigma_3=0;\ \lambda_1=\lambda,\ \lambda_2=1,\ \lambda_3=\lambda_{th}$), the stress difference equation (2) takes on the form of equation (11):

$$\frac{\sigma_{s-bi}\lambda}{\lambda^2-1/\lambda^2}=2W_1+2W_2 \quad (11)$$

By plotting $\sigma_{s-bi}\lambda$ against (λ^2-1/λ^2), one can use data fitting with the linear trendline and determine the summation $(2W_1+2W_2)=\mu$ from the slope of the linear trendline, but $2W_1$ and $2W_2$ cannot be determined separately from the plot.

The exact value of the slope at $\lambda\to 1$ can be calculated by expanding equation (11) as shown in equation (12):

$$\frac{\sigma_{s-bi}\lambda}{\lambda^2-1/\lambda^2}\xrightarrow[\varepsilon\to 0]{\lambda\to 1}\frac{\overbrace{\left(\frac{\varepsilon E}{1-\nu^2}\right)}^{\sigma_{s-bi}}(1+\varepsilon)}{(1+\varepsilon)^2-(1+\varepsilon)^{-2}}=\frac{\frac{\varepsilon}{1-\nu^2}\overbrace{2\mu(1+\nu)}^{E}\varepsilon(1+\varepsilon)}{(1+2\varepsilon+...)-(1-2\varepsilon+...)}\xrightarrow[\varepsilon^2\text{neglected}]{\nu=0.5}\frac{4\mu\varepsilon}{4\varepsilon}=\mu \quad (12)$$

The value of μ given by equation (12) is equal to the slope $(2W_1+2W_2)$ of the data-fitting linear trendline at $\lambda\to 1$.

Energy Method for Finding Material Constants

The energy method uses strain energy density plots to determine material constants $\{W_1,W_2\}$. After the stress-strain data are obtained, one can calculate the strain energy density W [(in-lb)/in^3] by integrating the area under the stress-strain curve up to any strain ε as described by equation (13):

$$W = \int_0^{\varepsilon} \sigma \, d\varepsilon \approx \sum_{k=1}^{m} \left(\frac{\sigma_k + \sigma_{k-1}}{2} \right) (\varepsilon_k - \varepsilon_{k-1}) = \sum_{k=1}^{m} \left(\frac{\sigma_k + \sigma_{k-1}}{2} \right) (\lambda_k - \lambda_{k-1}) \qquad (k = 1, 2, 3, ..., m) \tag{13}$$

In equation (13), σ can be $\sigma = \sigma_{uni}$, or $\sigma = \sigma_{e-bi}$, or $\sigma = \sigma_{s-bi}$. When $k = 1$, one has $\lambda_{k-1} = \lambda_0 = 1$ and $\sigma_{k-1} = \sigma_0 = 0$.

By plotting W against $(J_1 - 3)$, one can determine $W_1 \equiv \partial W / \partial J_1 \approx \Delta W / \Delta J_1$ from the slope of the linear trendline of the plotted data points. Likewise, by plotting W against $(J_2 - 3)$, one can determine $W_2 \equiv \partial W / \partial J_2 \approx \Delta W / \Delta J_2$ from the slope of the linear trendline of the plotted data points.

As will be seen shortly in the graphical presentations, the data points of energy plots are less scattered and almost linear, and therefore, can provide more accurate values of $\{W_1, W_2\}$ as compared with the values of $\{W_1, W_2\}$ determined by using stress-diffence plots.

Curve-Fitting Method for Finding Material Constants

The curve fitting method uses MSC-MARC® software (ref. 5) for curve fitting the experimental stress-strain data to obtain the material constants $\{W_1, W_2\}$ (special cases of Mooney constants). MSC-MARC® is a general-purpose finite element program for solving nonlinear problems. MSC-MARC® has been widely used by industry including auto, aero, biomedical, civil, electronics, shipbuilding, oil, gas, et cetera. MSC-MARC® provides a user friendly graphical user interface (GUI) called Mentat for curve fitting of the experimental data. The curve fitting procedure in Mentat is described in the followings curve-fitting procedure:

1. Create a new database in Mentat.
2. Read in the experimental data (uniaxial).
3. Read in the experimental data (biaxial).
4. Under the Material Properties tab, choose the experimental data fit.
5. Select experiment data type (uniaxial or biaxial).
6. Choose elastomer.
7. Choose Mooney−2 terms.
8. Select uniaxial, biaxial, or both.
9. Choose compute to calculate the coefficients (Mooney-Rivlin constants); $C_{10} (= W_1)$ and $C_{01} (= W_2 / J_3^2)$ (refs. 2, 3). For incompressible materials $(J_3 = 1)$; $C_{01} = W_2$.

Purpose of Experiments

The purpose of the experiments is to derive which analytical method is best for characterization of the room-temperature material behavior of the silicone rubber, the potential candidate material for aerospace applications. The experiments were carried out at Armstrong Flight Research Center (AFRC) Flight Loads Laboratory (FLL) (Edwards, California).

The material constants $\{W_1, W_2\}$ of any hyperelastic material should be unique and can be used to theoretically describe material behavior in any stress field. However, the earlier experiments of different hyperelastic materials by Blatz-Ko (refs. 2, 3) showed that the values of $\{W_1, W_2\}$ determined from uniaxial, equal-biaxial, and strip-biaxial tensile tests were somewhat different. Such stress-field dependent values of $\{W_1, W_2\}$ can be attributed to the molecular-chains crystallizations, which occur significantly less in a biaxial stress field than in a uniaxial stress field (ref. 4). The reason for the molecular-chains

crystallizations may be that the molecular chains cannot as easily form a regular lattice in biaxial stretching as in the case of uniaxial stretching where two degrees of freedom are available for lateral contractions.

Therefore, in the current material characterization of the silicon rubber test specimen, uniaxial, equal-biaxial, and strip-biaxial tensile tests were conducted. The resulting stress-stretch data were then used to determine the material constants $\{W_1, W_2\}$ of the silicone rubber test specimen by using the trendline method on stress-difference plots, modified stress-difference plots, energy plots, and the MSC-MARC® curve fitting method based on the experimental stress-stretch data. The values of $\{W_1, W_2\}$ determined from uniaxial, equal-biaxial, and strip-biaxial tensile tests were then compared, and universal values of $\{W_1, W_2\}$ were established based on the new equal-biaxial energy plots.

Descriptions of Uniaxial Experiments

The uniaxial tensile tests were performed first. The resulting stress-stretch data were re-plotted as stress-difference plots to determine the material constants $\{W_1, W_2\}$ for the silicone rubber. The values of $\{W_1, W_2\}$ determined from uniaxial tensile tests will then be compared with the values of $\{W_1, W_2\}$ determined from equal-biaxial and strip-biaxial tensile tests, and the difference in the values of $\{W_1, W_2\}$ will be examined.

Uniaxial Specimen-Gripping Method

In the uniaxial tensile tests of the current silicone rubber material, the specimen can be stretched up to nearly ten times the original length (that is, extension ratio $\lambda \to 10$). In the uniaxial tensile tests of hyperelastic materials, the big problems are: 1) Pulling out of the specimen ends from the gripping jaws before true failure extension ratio can be reached because the stretched specimen becomes thinner at large extensions, and 2) Premature failure because of stress concentration induced by overgripping. The gripping jaws with wavy surfaces can improve the gripping efficiency, enabling the specimen to reach higher extension ratios. However, the gripped specimen ends will eventually slip off the gripping jaws before reaching the true failure extension ratio.

After testing of various gripping methods to prevent the specimen from slipping, the specimen-gripping method shown in figure 1 was invented. The test region of the uniaxial test specimen has the dimensions of length (*l*), width (*w*), and thickness (*t*) listed in table 1.

Table 1. Dimensions of uniaxial tensile test specimen.

l, in. (Test length)	*w,* in. (Width)	*t*, in. (Thickness)
5.0	1.0	0.03

The length of the original flat specimen before end folding is 11 in. Each end of a three-inch-long region is wrapped around a transverse short silicone rubber stick, folded with interface, and bonded using Dow Corning 3145 clear silicone adhesive (Dow Corning Corporation, Midland, Michigan) to form a double-layer gripping region (1.5 in.) with a bulged end, leaving a five-inch test region. Thus, by using self-tightening scissor grip clamps (fig.1) to keep up with the change in the specimen thickness under tension, each bulged end will function as a stop to prevent the specimen from slipping out of the grip clamps, enabling the specimen to reach a very large extension ratio λ around λ=10 causing the specimen to fail at its middle region. This innovative method completely eliminated the specimen-slipping problem.

Uniaxial Tensile Tests

Figure 2 shows the uniaxial tensile test setups. The gripped uniaxial specimen before loading is shown on the left, and the retracted specimen after stretching up to extension ratio $\lambda = 8$ is shown on the right. Note that the surface of the uniaxial test specimen is marked with either transverse marking lines or black grid points so that the extension ratio can be measured by a photogrammetry system (left side of fig. 2). The photogrammetry system could provide accurate deformation data up to extension ratio $\lambda = 3$, beyond which the reading accuracy degraded due to contrast degradation of the target pattern as the specimen was stretched. Therefore, for large extensions beyond $\lambda = 3$, the measurement method had to be changed to a video image pixel measurement method.

Each virgin specimen was repeatedly stress-cycled (stretched up to extension ratio $\lambda \approx 6$) until the final steady-state stress-strain data could be obtained. Between each stress cycling, a one-hour duration was allowed for the retracted specimen to relax before the next loading cycle. However, the stress-cycled specimen never retracted completely to its original length, leaving a hysteresis of nearly 0.5-in. (10 percent of the specimen original length, l = 5 in.).

Figure 3 shows a typical set (Coupon 6) of uniaxial stress-stretch data associated with different number of stress cyclings. Note from figure 3 that the virgin (first stress cycle) and subsequent stress-cycled stress-stretch curves are marked different (especially between the initial three cycles), indicating a high degree of material sofetening after each stress cycling. Note also that the stress-stretch curve finally reached steady state at the fifth stress cycle. The fifth stress cycles of stress-stretch data of both Coupon 5 and Coupon 6 were then used to determine the material constants $\{W_1, W_2\}$.

Descriptions of Radial-Biaxial Experiments

The purpose of radial-biaxial tests is to obtain equal-biaxial stress-stretch data for determining the material constants $\{W_1, W_2\}$ for comparison with the values of $\{W_1, W_2\}$ determined from uniaxial tensile tests. Keep in mind that the molecular-chains crystallization occurring in a biaxial stress field is significantly less than that occurring in a uniaxial stress field (ref. 4).

Radial-Biaxial Tester

Figures 4 show the design concept (fig. 4(a)) and actual top view (fig. 4(b)) of the low-cost hand-operated five-foot-diameter round table of the radial-biaxial tester constructed at AFRC-FLL. The radial-biaxial tester [under the National Aeronautics and Space Administration (NASA) New Technology Reporting (NTR) protection DRC-017-007] is capable of stretching the circular specimen up to the design-limit radial (= tangential) extension ratio of $\lambda = 4$. The circular specimen of the FLL silicon rubber used in the radial-biaxial tests has a radius of b = 5 in. and a thickness of t = 0.03 in. The circular specimen boundary is to be radially pulled by n = 32 equally spaced pulling strings to induce an equal-biaxial stress field everywhere in the circular specimen (that is, radial and tangential stresses are identical). The surface of the round table is marked with concentric circles of different radii $\overline{b}$ (= 6.25, 7.50, 8.75, 10.00, 11.25, 12.50, 13.75, 15.00, 16.25, 17.50, 18.75, 20.00) to indicate different radial extension ratios of $\lambda \equiv \overline{b}/b$ (= 1.25, 1.50, 1.75, 2.00, 2.25, 2.50, 2.75, 3.00, 3.25, 3.50, 3.75, 4.00) for the deformed specimen boundary to match when the circular specimen is radially pulled by n = 32 equally spaced pulling strings. The outer ends of the pulling strings are connected to 32 tangentially arrayed miniature hand winches, which are anchored at the periphery of the round table. Because of the axisymmetric nature, only four miniature tensile meters were installed at four tangential locations (0, 90, 270, 360) deg to record the total sum of the four pulling string tension ($4T$), from which the averaged individual pulling string tension T can be obtained.

Specimen Boundary Geometries

For radial pulling of the specimen, two types of specimen boundary geometries were used:

1. Gear-shaped specimen (fig. 5): Boundary of the gear-shaped specimen has n = 32 pulling tongues for connection to 32 pulling strings; and
2. Smooth specimen (fig. 6): Boundary of the smooth specimen has n = 32 equally spaced pulling stations for connection to 32 pulling strings.

Specimen Bonding Methods

After performing various types of specimen bonding strength tests, the best specimen bonding methods for pulling the test specimens [gear-shaped (fig. 5) and smooth (fig. 6)] were found to be the types shown in figures 5 and 6. For resisting the pulling string force without bonding failure, both ends of the webbing loop (shoelace like strap) were bonded with Dow Corning 3145 clear silicone adhesive to both sides of the specimen boundary pulling station (figs. 5 and 6). To maximize the break-away strength at the attachment, each bonded site (lower or upper) was covered and bonded with an extra layer of the elastomer (figs. 5 and 6). This reinforcing approach could nearly double the ultimate break-away strength.

Pre-Test Estimation of Pulling-String Tension

Before the radial-biaxial tensile tests can be carried out, one needs to theoretically estimate the range of the pulling string tension T so that proper tensile meters could be selected. One can use the material constants (W_1= 7.5, W_2 = 2.0) lb/in^2 determined from the uniaxial tensile tests to calculate the estimated values of T from equation (14) (see Appendix A):

$$T = \left(\frac{2\pi bt}{n} \right) \sigma_{e-bi} \tag{14}$$

In equation (14), the theoretical engineering equal-biaxial stress σ_{e-bi} at the specimen boundary can be calculated from equation (7).

In view of equations (14) and (7), the predicted tensile force T in each pulling string can be expressed in the form of equation (15):

$$T = \left(\frac{2\pi bt}{n} \right) \underbrace{\left[\left(2W_1 + 2W_2\lambda^2 \right) \left(\lambda - \frac{1}{\lambda^5} \right) \right]}_{\sigma_{e-bi}} \tag{15}$$

The calculated theoretical biaxial stress σ_{e-bi} and the estimated pulling string tension T are listed in table 2.

Table 2. Estimated equal-biaxial stress σ_{e-bi} and pulling-string tention T calculated respectively from equations (7) and (15) using uniaxial material constants (W_1= 7.5, W_2 = 2.0) lb/in^2; (b = 5.0 in., t = 0.03 in., n = 32).

$\sigma_{e-bi} = \left(2W_1 + 2W_2\lambda^2\right)\left(\lambda - \frac{1}{\lambda^5}\right)$		$T = \left(\frac{2\pi bt}{n}\right)\sigma_{e-bi}$
λ	σ_{e-bi}, lb/in^2	T, lb
1.00	0.0000	0.0000
1.25	19.5993	0.5248
1.50	32.8395	0.8793
1.75	46.0272	1.2324
2.00	61.0313	1.6341
2.50	78.7012	2.1072
2.25	99.5904	2.6665
2.50	124.1498	3.3241
3.00	152.7901	4.0909
3.25	185.9046	4.9775
3.50	223.8781	5.9942

Note from table 2 that the required pulling string tension T is relatively low, only $T = 5.9942$ lb at λ = 3.5. Data in table 2 were then used to select the size of the tensile meters for measuring the actual pulling string tension T.

Figure 7 shows the pre-test estimated pulling string tension T (table 2) required to pull a circular sheet (b = 5 in., t = 0.03 in.) of the silicon rubber specimen to the desired radial extension ratio λ for the selection of tensile meters.

Figures 8 and 9 respectively show the overall view and the close-up view of the Radial-Biaxial Tester constructed at the NASA Armstrong Flight Research Center Flight Loads Laboratory. The circular specimen (b = 5.0 in., t = 0.03 in.) is radially pulled by an n = 32 miniature hand winch anchored at the periphery of the round table. As mentioned earlier, the Radial-Biaxial Tester is for material characterization under an equal-biaxial stress field, and is capable of stretching the specimen up to the design-limit radial extension ratio of $\lambda(\equiv \bar{b}/b) = 4$.

Radial-Biaxial Tests

As shown in figure 10, the Radial-Biaxial Tester is manually operated. The circular specimen was radially pulled step-by-step by using two people to manually turn the two hand winches located at diametrically opposite sides (180 deg apart) of the round table. When the specimen boundary points along this particular diameter reached a certain circular marking of radius $\bar{b}$ on the round table, indicating the desired radial extension ratio $\lambda(=\bar{b}/b)$, a similar pulling process was repeated for the next neighboring diameter, and so on. When all the n = 32 winches were turned so that the specimen boundary was stretched to nearly the desired radial extension ratio λ, fine tuning of pulling force adjustments were made by observing the image of the deformed specimen displayed on the viewing screen (fig. 11) generated by the overhead camera, until the specimen boundary matched perfectly a particular circular ring marking (radius = $\bar{b}$) on the round table, giving the desired radial extension ratio λ.

Figures 12(a), 12(b), 13(a), and 13(b) show the undeformed (a) and deformed (b) states of the two types of radial-biaxial tensile test specimens on the round table of the radial-biaxial tester. Note from figures 12 and 13 that in addition to the original tensile meters at tangential locations (0, 90, 270, 360) deg, eight additional tensile meters of different types were added to record the pulling string tension T. The load

outputs from those eight additional tensile meters, however, were questionable, and therefore, only the data from the original four tensile meters were used to obtain the desired pulling string tension *T*.

1. Stress Cycling

Each specimen (gear-shaped boundary or smooth boundary) was repeatedly tested for six cycles to obtain a family of biaxial stress-stretch curves. Between each stress cycling, one-hour duration was allowed for the retracted specimen to relax before the next loading cycle. However, the pre-tested specimen never retracted completely to its original radius (b = 5 in.), leaving hysteresis of nearly 0.5 in. (10 percent radial elongation). The relaxed radius b = 5.5 in. was then used as the new undeformed radius for modifying the original reading of radial extension ratios λ based on the radii $\overline{b}$ of the round table concentric circular markings which are in reference to the original undeformed radius b = 5 in.

2. Equal-Biaxial Stress Calculations

Because there are no large-deformation stress sensors to accurately sense the equal-biaxial engineering stress σ_{e-bi}, the measured pulling string tension T was used to calculate σ_{e-bi}. Under a fixed radial extension ratio λ, the rubber specimen will relax, causing the pulling string tension T to decrease with time to a fully relaxed value in about 5 minutes (refs. 6, 7). Then, in view of equation (14), the fully relaxed value of the pulling string tension $T(\lambda)$ at λ can then be used to calculate the induced equal-biaxial engineering stress $\sigma_{e-bi}(\lambda)$ at λ from equation (16).

$$\sigma_{e-bi}(\lambda) = \frac{nT(\lambda)}{2\pi bt} \tag{16}$$

Equation (16) will then be used to calculate the experimental equal-biaxial stress-stretch curves.

Figures 14 show typical sets of equal-biaxial stress-stretch curves associated with a different number of stress cyclings using a gear-shaped specimen (fig. 14(a)) and a smooth specimen (fig. 14(b)). Note from figures 14 that the virgin (first stress cycling) and subsequent stress-cycled stress-stretch curves are very different, indicating a high degree of material sofetening after the first stress cycling. The subsequent stress-cycled stress-stretch curves are quite close and were then used to determine the material constants $\{W_1, W_2\}$.

Descriptions of Strip-Biaxial Experiments

Because the molecular-chains crystallization (alignment of polymer molecular chains due to stretching) occurring in the biaxial stress field is significantly less than that occurring in the uniaxial stress field (ref. 3), values of material constants $\{W_1, W_2\}$ must also be examined in the strip-biaxial stress field. As mentioned earlier, from the strip-biaxial tensile tests, one can only determine the summation of the material constants $(W_1 + W_2)$ [see equation (11)], but not W_1 and W_2 separately. The purpose of strip-biaxial tests is then to obtain strip-biaxial stress-stretch data for determining the summation of material constants $(W_1 + W_2)$ for comparison with the values of $(W_1 + W_2)$ determined from both uniaxial and equal-biaxial tensile tests.

Strip-Biaxial Specimen-Gripping Method

The test region of the strip-biaxial test specimen has the dimensions (length l, width w, and thickness t) listed in table 3.

Table 3. Dimensions of the uniaxial tensile test specimen.

l, in. (Test length)	*w,* in. (Width)	*t*, in. (Thickness)
1.0	7.0	0.03

The surface of each strip-biaxial test specimen was marked with horizontal grid lines so that the extension ratio can be measured by either a measuring tape or by a video camera system.

Figure 15 shows the strip-biaxial (laterally constrained uniaxial) tensile test system developed at AFRC-FLL to obtain stress-stretch data for determinations of material constants summation $(W_1 + W_2) = \mu/2$. Note the innovative gripping method for the strip-biaxial test specimen. The length of the original flat silicon rubber sheet for the strip-biaxial specimen is three inches, allowing on each side a one-inch-wide horizontal edge region that is sandwiched and bonded between the folded gripping silicon rubber sheet (0.085 in. thick), thus leaving *l* = one-inch test region. The folded gripping silicon rubber sheet is wrapped around a seven-inch reinforcing metal rod to form a bulged edge. To generate a true strip-biaxial stress field in the specimen test region, metal sheets are bonded to the surfaces of the folded silicone rubber gripping regions for maintaining straight gripping edges (fig. 15).

When axially loaded, each bulged edge will function as a stop to prevent the specimen from slipping through the scissor-shaped grips with embodied horizontal slip-resisting steel rods (fig. 15). The innovative specimen-gripping method mentioned above totally eliminated the specimen-slipping problem.

To prevent the specimen two vertical free-edges from contraction (cave in) under loading, another innovative simple method was developed at the AFRC FLL. Namely, by bonding both ends of the contraction-constraint wooden rods to the two vertical free edges with silicone adhesive (fig. 15), lateral contraction can be constrained to maintain zero lateral strain.

Strip-Biaxial Tests

Figures 16 show the strip-biaxial tensile test specimen before (fig. 16(a)) and after (fig. 16(b)) deformation. Notice that the lateral contraction of the two vertical edges can be effectively constrained to maintain zero lateral stretch (that is, $\lambda_2 = 1$) at the constraining wooden rods attachment points.

Each virgin specimen was repeatedly stress-cycled (stretched up to the extension ratio $\lambda = 4$ until the final steady-state stress-stretch data could be obtained. Between each stress cycling, a one-hour duration was allowed for the retracted specimen to relax before the next loading cycle. However, the stress-cycled specimen never retracted completely to its original length, leaving a hysteresis of nearly 0.03125 in. (3.125 percent of specimen original length *l* = 1 in.).

Figure 17 shows a typical set of strip-biaxial stress-stretch data associated with a different number of stress cyclings. Note from figure 17 that the virgin (first stress cycle) and subsequent stress-cycled stress-stretch curves are marked different, indicating a high degree of material sofetening after each stress cycling. The final 13th stress-cycled stress-stretch data were then used for the stress-difference plot for determination of the material constants $\{W_1 + W_2\}$.

Data Reductions-Determinations of Material Constants

The following sections describe different methods for re-plotting the uniaxial and biaxial stress-stretch data for graphically determining the material constants $\{W_1, W_2\}$ or material constants summation $(W_1 + W_2)$ for the silicon rubber using the trendline method on stress-difference plots, modified stress-difference plots, and energy plots. The results will be compared with the corresponding values of $\{W_1, W_2\}$ obtained from the MSC-MARC® direct curve fitting methods.

Uniaxial Case

Figure 18 shows the fifth-cycle (steady state) uniaxial stress-stretch data of Coupon 5 and Coupon 6, which were used in the determination of the material constants $\{W_1, W_2\}$ for the silicon rubber. The stress-stretch data shown in figure 18 were re-plotted in different ways so that the values of $\{W_1, W_2\}$ can be determined graphically using the linear trendline method.

1. Uniaxial Type-1 Plots

Figure 19 shows the uniaxial Type-1 plots based on the stress-difference equation (3) fitted with a linear trendline for determining material constants $\{W_1, W_2\}$. The intercept of the trendline at $1/\lambda = 0$ gives $2W_1 = 15$ lb/in^2, and the intercept at $1/\lambda = 1$ gives $2(W_1 + W_2) = \mu = 19$ lb/in^2, resulting in the values of $(W_1 = 7.5, W_2 = 2.0)$ lb/in^2 for the FLL silicone rubber. The MSC curve-fitting method also yields comparative values of $(W_1 = 7.513, W_2 = 2.179)$ lb/in^2.

2. Uniaxial Type-2 Plots

Figure 20 shows the uniaxial Type-2 plots based on the modified stress-difference equation (4) fitted with a linear trendline for determining material constants $\{W_1, W_2\}$. Notice that the Type-2 plots are less wavy than uniaxial Type-1 plots (fig. 19). The intercepts of the trendline at $1/\lambda = 0$ gives $2(W_1 + W_2) = \mu = 19$ lb/in^2, and the slope of the trendline gives $2W_1 = 15$ lb/in^2, from which one obtains $(W_1 = 7.5, W_2 = 2.0)$ lb/in^2 for the silicone rubber. The MSC-MARC® curve-fitting method also gives comparative values of $(W_1 = 7.513, W_2 = 2.179)$ lb/in^2.

3. Uniaxial Energy Plots

Figure 21 shows the plots of uniaxial strain energy density data of *W* for the silicone rubber as functions of $(J_1 - 3)$, the shifted first invariant of the Cauchy-Green deformation tensor. The plots are almost linear with the averaged slope of $W_1 = 8.0$ lb/in^2, which is comparable to the values of $(W_1 = 7.5;\ W_1 = 7.513)$ lb/in^2 determined respectively from the stress-difference plots and MSC-MARC® curve-fitting method.

Figure 22 shows the plot of uniaxial strain energy density data of *W* for the silicone rubber as a function of $(J_2 - 3)$, the shifted second invariant of the Cauchy-Green deformation tensor. The plots are less linear, and the linear trendline gives the averaged slope of $W_2 = 24.40$ lb/in^2, which is more than ten times the values of ($W_2 = 2.00$; $W_2 = 2.179$) lb/in^2 determined respectively from the stress-difference plots and MSC-MARC® curve-fitting method. The unrealistic value of $W_2 = 24.4$ lb/in^2 can be attributed to the small range of $J_2 (= 1/\lambda^2 + 2\lambda)$ in the plot of *W* against $(J_2 - 3)$ (fig. 22) in the uniaxial deformations (see the Comments on Energy Plots section). As will be seen shortly, the correct value of W_2 can be determined from the equal-biaxial stress field.

4. Uniaxial Data Summary

The material constants $\{W_1, W_2\}$ for the silicon rubber determined from uniaxial tensile tests are listed in table 4.

Table 4. Material constants $\{W_1, W_2\}$ for the silicon rubber determined from uniaxial tensile tests (l = 5 in., w = 1 in., t = 0.03 in.).

	W_1, lb/in^2	W_2, lb/in^2
Stress-difference plots (Type 1, Type 2)	7.500	2.000
MSC curve fitting	7.513	2.179
Energy plots	8.000	24.400*

* Unrealistic value

Notice from table 4 that the values of $\{W_1, W_2\}$ determined using the trendline method and the MSC curve-fitting method are very close, giving the confidence in the two approaches for the determinations of $\{W_1, W_2\}$. The energy method gives the reasonable value of $W_1 = 8.00$ lb/in^2, but an unrealistic large value for $W_2 = 24.4$ lb/in^2. Therefore, the energy method should not be used to determine W_2 from the uniaxial data (see the Comments on Energy Plots section).

5. Uniaxial Graphical Presentations

Based on $(W_1 = 7.5, W_2 = 2.0)$ lb/in^2 (stress-difference plots) and $(W_1 = 7.513, W_2 = 2.179)$ lb/in^2 (MSC curve-fitting) listed in table 4, the theoretical stress-stretch curves can be calculated from equation (17) [a rewritten form of equation (3)]:

$$\sigma_{uni} = \left(2W_1 + \frac{2W_2}{\lambda}\right)\left(\lambda - \frac{1}{\lambda^2}\right) \tag{17}$$

Figure 23 compares the experimental uniaxial stress-stretch curves with the theoretical stress-stretch curves calculated from equation (17). Note that the two theoretical stress-stretch curves are very close and can describe the uniaxial stress-strain behavior of the silicon rubber fairly well up to $\lambda \approx 5$.

Equal-Biaxial Case

The stress-cycled biaxial stress-stretch data (stress cycles 2-6) shown in figures 24(a) and 24(b) were used in the determination of the equal-biaxial material constants $\{W_1, W_2\}$ for FLL silicon rubber. Figures 24(a) and 24(b) are actually figures 14(a) and 14(b) with virgin stress-stretch curves (first stress-cycle) removed because, the initial stress curve for the virgin material is far off from the subsequent stress curves of cycles 2-6. The stress-stretch data shown in figures 24 were then re-plotted in different types of plots for graphical determinations of the material constants $\{W_1, W_2\}$ using the linear trendline data fittings.

1. Equal-Biaxial Type-1 Plots

Figures 25 show the equal-biaxial Type-1 plots based on the stress-difference equation (7) fitted with a linear trendline for determining the material constants $\{W_1, W_2\}$. Notice that equal-biaxial Type-1 plots are slightly wavy, and all the curves for different tests are not very cohesive.

For the gear-shaped case (fig. 25(a)), the intercept of the trendline at $1/\lambda = 0$ gives $2(W_1 + W_2) = \mu =$ 25 lb/in^2, and the slope of the trendline gives $2W_1 = 1.5$ lb/in^2, resulting in the material constants of $(W_1 = 11.75, W_2 = 0.75)$ lb/in^2 for the silicone rubber.

For the smooth case (fig. 25(b)), the intercept of the trendline at $1/\lambda = 0$ gives $2(W_1 + W_2) = \mu =$ 25.2 lb/in^2, and the slope of the trendline gives $2W_1 = 1.2$ lb/in^2, from which the material constants are obtained as $(W_1 = 12.0, W_2 = 0.6)$ lb/in^2 for the silicone rubber.

2. Equal-Biaxial Type-2 Plots

Figures 26 show the equal-biaxial Type-2 plots based on the modified stress-difference equation (8) fitted with a linear trendline for determining the material constants $\{W_1, W_2\}$ for the silicone rubber.

For the gear-shaped case (fig. 26(a)), except for small strain regions where data are scattered, in the large extension region $(0.1 < 1/\lambda^2 < 0.4)$, the equal-biaxial Type-2 curves form almost straight bands, which can be fitted with a linear trendline. The intercept of the trendline at $1/\lambda = 0$ gives $2(W_1 + W_2) = \mu = 25$ lb/in^2, and the slope of the trendline gives $2W_1 = 1.5$ lb/in^2, resulting in the material constants of $(W_1 = 11.75, W_2 = 0.75)$ lb/in^2 for the silicone rubber.

For the smooth case (fig. 26(b)), in the large extension region $(0.1 < 1/\lambda^2 < 0.5)$, the equal-biaxial Type-2 curves also form cohesive straight bands, which can be fitted with a linear trendline. The intercept of the trendline at $1/\lambda = 0$ gives $2(W_1 + W_2) = \mu = 25.2$ lb/in^2, and the slope of the trendline gives $2W_1 = 1.2$ lb/in^2, from which the material constants are obtained as $(W_1 = 12.0, W_2 = 0.6)$ lb/in^2 for the silicone rubber.

3. Equal-Biaxial Data Summary

The values of $\{W_1, W_2\}$ determine from the stress-difference plots, and the values of $\{W_1, W_2\}$ determined from the MSC-MARC® curve-fitting method for the silicon rubber are listed in table 5 for comparisons.

Table 5. Material constants $\{W_1, W_2\}$ for the silicon rubber determined from radial-biaxial tensile tests using stress-difference plots and MSC-MARC® curve fitting; b = 5 in., t = 0.03 in.

	Stress-difference plots		MSC curve fitting	
Case	W_1, lb/in^2	W_2, lb/in^2	W_1, lb/in^2	W_2, lb/in^2
Gear-shaped boundary	11.75	0.75	11.32	1.02
Smooth boundary	12.00	0.60	13.18	0.64
Average	11.88	0.68	12.25	0.83

Note that the values of $\{W_1, W_2\}$ determined from the two methods are relatively close.

After the material constants $\{W_1, W_2\}$ are determined from the radial-biaxial tests, one can now use the averaged material constants (W_1= 11.88, W_2 = 0.68) lb/in^2 listed in table 5 to calculate the actual pulling string tension T from equation (15). The actual values of the pulling string tension T are listed in the Actual Pulling-String Tension section.

4. Equal-Biaxial Energy Plots

Figures 27 show the plots of the equal-biaxial strain energy density data of W as a function of $(J_1 - 3)$, the shifted first invariant of the Cauchy-Green deformation tensor associated with the gear-shaped specimen (fig. 27(a)) and smooth specimen (fig. 27(b)). The data points fell within a narrow band, which is nearly linear with the averaged slope (trendline) of W_1 = (7.84; 7.833) lb/in^2 respectively for the gear-shaped specimen and smooth specimen.

Figures 28 show the plots of the equal-biaxial strain energy density of W as a function of $(J_2 - 3)$, the shifted second invariant of the Cauchy-Green deformation tensor. The plots are less linear, and the linear trendline gives the averaged slope of W_2 = (1.683; 1.667) lb/in^2 respectively for the gear-shaped specimen (fig. 28(a)) and smooth specimen (fig. 28(b)).

5. Equal-Biaxial Energy Data Summary

The material constants $\{W_1, W_2\}$ for the FLL silicon elastomer determined from the equal-biaxial stress-strain data using the biaxial energy method and the MSC combined curve fitting method (fitting both uniaxial and biaxial stress-strain data) are compared in table 6.

Table 6. Comparisons of material constants $\{W_1, W_2\}$ of the silicon rubber determined from the equal-biaxial energy plots and the MSC uniaxial/biaxial combined curve fitting.

	Equal-biaxial energy plots		MSC combined curve fitting	
Case	W_1, lb/in^2	W_2, lb/in^2	W_1, lb/in^2	W_2, lb/in^2
Gear-shaped boundary	7.844	1.683	7.784	1.712
Smooth boundary	7.833	1.667	7.837	1.709
Average	7.839	1.675	7.811	1.711

Note from table 6 that the material constants $\{W_1, W_2\}$ determined using the equal-biaxial energy-plots turned out to be very close to the values of $\{W_1, W_2\}$ determined from the MSC-MARC® combined curve fitting of both uniaxial and biaxial stress-stretch data. Thus, the values of $\{W_1, W_2\}$ determined from the equal-biaxial energy plots and from the MSC-MARC® combined curve fitting can be considered as the universal material constants for establishing the theoretical constitutive equations for both uniaxial and equal-biaxial stress fields.

6. Equal-Biaxial Graphical Presentations

Based on different values of $\{W_1, W_2\}$ listed in table 5 and table 6, the theoretical equal-biaxial stress-stretch curves for the silicone rubber can be calculated from equation (18) [rewritten form of equation (7)]:

$$\sigma_{e-bi} = \left(2W_1 + 2W_2\lambda^2\right)\left(\lambda - \frac{1}{\lambda^5}\right) \tag{18}$$

Figures 29(a) and 29(b) compare the experimental equal-biaxial stress-stretch curves with the theoretical equal-biaxial stress-stretch curves based on different sets of the material constants $\{W_1, W_2\}$. Overall, the comparison is fairly good considering the scattering of the experimental data.

Strip-Biaxial Case

Figure 30 shows the experimental strip-biaxial stress-stretch curve (stress-cycle 13 of figure 17), which is used in the following stress-difference plots for graphical determinations of the material constants summation $(W_1 + W_2)$.

1. Stress-Differential Plots

Based on equation (11), the data of figure 30 were re-plotted in figure 31 as the strip-biaxial stress-difference plot for fitting with a linear trendline. From the slope of the trendline, the summation of the material constants can be determined as $(W_1 + W_2) = 8.25$ lb/in^2 for the FLL silicone rubber.

2. Strip-Biaxial Energy Plots

Figure 32 shows the plots of strip-biaxial strain energy density data of W as functions of $(J_1 - 3)$, the shifted first invariant of Cauchy-Green deformation tensor. The data points practically form a linear line

with the averaged slope (trendline) of $W_1 = 7.97$ lb/in^2. Because $(J_2 - 3) = (J_1 - 3)$ for the strip-biaxial stress field, one obtains $W_2 = W_1 = 7.97$ lb/in^2 (see the Comments on Energy Plots section).

3. Strip-Biaxial Data Summary

The material constants $\{W_2, W_1\}$ for the silicon rubber determined from strip-biaxial tensile tests are listed in table 7.

Table 7. Material constants $\{W_1, W_2\}$ for the silicon rubber determined from strip-biaxial tensile tests (l = 1 in., w = 7 in., t = 0.03 in.).

Plot type	W_1, lb/in^2	W_2, lb/in^2	$(W_1 + W_2)$, lb/in^2
Stress-difference plots	------	------	8.25
MSC curve fitting	4.06	4.06	8.12
Energy plots	7.97	7.97	15.94

Note from table 7 that the strip-biaxial energy plot gives $W_1 = 7.97$ lb/in^2, which is comparable to the values of $W_1 = 8.00$ lb/in^2 (uniaxial case, table 4) and $W_1 = 7.839$ lb/in^2 (equal-biaxial case, table 6). However, the value of $W_2 = W_1 = 7.97$ lb/in^2 determined from the trip-biaxial energy plot is somewhat questionable (see the Comments on Energy Plots section).

4. Strip-Biaxial Graphical Presentations

Figures 33(a) and 33(b) compare the experimental strip-biaxial stress-stretch curves with the theoretical curves calculated from equation (19) [a rewritten form of equation (11)] using the value of $(W_1 + W_2) = 8.25$ lb/in^2 (stress-difference plot) and $(W_1 + W_2) = 8.12$ (MSC curve fitting):

$$\sigma_{s-bi} = (2W_1 + 2W_2)\left(\lambda - \frac{1}{\lambda^3}\right) \tag{19}$$

Note that the two theoretical stress-stretch curves are very close and can describe the strip-biaxial stress-strain behavior of the silicon rubber fairly well up to λ = 4.25.

Final Summary of Experientially Determined Material Constants

All the material constants $\{W_1, W_2\}$ determined for the silicon rubber listed in tables 4-7 are combined into table 8 for easy comparison of the values of $\{W_1, W_2\}$.

Table 8. Final summary of material constants $\{W_1, W_2\}$ for the silicon rubber determined from uniaxial, equal-biaxial, and strip-biaxial tensile tests.

Uniaxial case			
Plot type	W_1, lb/in^2	W_2, lb/in^2	$(W_1 + W_2)$, lb/in^2
Stress-difference plots	7.500	2.000	9.500
MSC curve fitting	7.513	2.179	9.692
Uniaxial energy plots	8.000	24.400	32.400
Equal-biaxial case (Gear and smooth cases averaged)			
Plot type	W_1, lb/in^2	W_2, lb/in^2	$(W_1 + W_2)$, lb/in^2
Stress-difference plots	11.880	0.680	12.560
MSC curve fitting	12.250	0.830	13.180
Equal-biaxial energy plots	7.839	1.675	9.514
Strip-biaxial case			
Plot type	W_1, lb/in^2	W_2, lb/in^2	$(W_1 + W_2)$, lb/in^2
Stress-difference plots	------	------	8.25
MSC curve fitting	4.06	4.06	8.12
Strip-biaxial energy plots	7.97	7.97	15.94
Universal case (Gear and smooth cases averaged)			
Plot type	W_1, lb/in^2	W_2, lb/in^2	$(W_1 + W_2)$, lb/in^2
Equal-biaxial energy plots	7.839	1.675	9.514
MSC combined curve fitting	7.811	1.711	9.522

Using the values of $(W_1 = 7.839, W_2 = 1.675)$ lb/in^2 (equal-biaxial energy plots) and $(W_1 = 7.811, W_2 = 1.711)$ lb/in^2 (MSC combined curve fitting) listed in table 8, two sets of theoretical stress-stretch curves were calculated from equations [(17), (18), and (19)] respectively for the uniaxial, equal-biaxial, and strip-biaxial stress fields.

Figure 34 shows the combined plots of the theoretical stress-stretch curves [eqs. (17), (18), and (19)] for different stress fields. The dark blue curves are based on $(W_1 = 7.839, W_2 = 1.675)$ lb/in^2 (equal-biaxial energy plots), and the dashed dark blue curves are based on $(W_1 = 7.811, W_2 = 1.711)$ lb/in^2 (MSC combined curve fitting). The two sets of the theoretical stress-stretch curves are extremely close and are compared with the associated uniaxial, equal-biaxial, and strip-biaxial tensile test data. Note that the theoretical stress-stretch curves based on just two material constants $\{W_1, W_2\}$, compare fairly well with the associated uniaxial, equal-biaxial, and strip-biaxial stress-stretch data. Therefore, the values of $\{W_1, W_2\}$ determined from equal-biaxial energy plots and from MSC combined curve fitting can be considered as the universal material constants for theoretically describing the mechanical behavior of the silicon rubber in any stress fields.

Comments on Energy Plots

The reason why the unrealistic values of W_2 determined from the uniaxial energy plots and strip-biaxial energy plots can be explained by observing the mathematical forms of $\{J_1, J_2\}$. The mathematical forms of $\{J_1, J_2\}$ written out for different stress fields for incompressible materials $(J_3 = \lambda_1 \lambda_2 \lambda_3 = 1)$ are listed in table 9.

Table 9. Mathematical forms of $\{J_1, J_2\}$ written out for uniaxial, equal-biaxial, and strip-biaxial stress fields for incompressible materials $(J_3 = \lambda_1\lambda_2\lambda_3 = 1)$.

Stress field	$J_3 = \lambda_1\lambda_2\lambda_3 = 1$	$J_1 = \lambda_1^2 + \lambda_2^2 + \lambda_3^2$	$J_2 = \frac{1}{\lambda_1^2} + \frac{1}{\lambda_2^2} + \frac{1}{\lambda_3^2}$
Uniaxial	$\lambda\lambda_{lat}^2 = 1$	$J_1 = \lambda^2 + \frac{2}{\lambda}$	$J_2 = \frac{1}{\lambda^2} + 2\lambda$
Equal-biaxial	$\lambda^2\lambda_{th} = 1$	$J_1 = 2\lambda^2 + \frac{1}{\lambda^4}$	$J_2 = \frac{2}{\lambda^2} + \lambda^4$
Strip-biaxial*	$\lambda \cdot 1 \cdot \lambda_{th} = 1$	$J_1 = \lambda^2 + 1 + \frac{1}{\lambda^2}$	$J_2 = \frac{1}{\lambda^2} + 1 + \lambda^2 = J_1$

* Note: $J_1 = J_2$

Note from table 9 that for all the three stress fields, J_1 has a dominant λ^2 term, causing the values of W_1 determined from the energy plots to be comparable. However, for the uniaxial case, J_2 has only λ term, causing the slope W_2 in the W against J_2 plot to be many times larger than the value of W_2 determined from equal-biaxial case, for which J_2 has λ^4 term, giving the correct value of W_2. Note also that, for the strip-biaxial case, $J_1 = J_2$, giving $W_2 = W_1$ in the energy plots. Thus, the energy plot should be limited to equal-biaxial stress field.

Actual Pulling String Tension

After the material constants $\{W_1, W_2\}$ are determined from the equal-biaxial tests, one can now use the averaged material constants (W_1= 11.88, W_2 = 0.68) lb/in^2 listed in table 5 to calculate the theoretical equal-biaxial stress σ_{e-bi}, from equation (18) and the theoretical pulling string tension T from equation (14). The results are listed in table 10.

Table 10. Theoretical equal-biaxial stress σ_{e-bi} and theoretical pulling-string tention T for pulling a circular specimen (post-cycled radius b = 5.5 in., post-cycled thickness t = 0.024793 in.)* to desired radial extension ratios λ using averaged equal-biaxial material constants (W_1= 11.88, W_2 = 0.68) lb/in^2 for the silicone rubber; n = 32.

$\sigma_{e-bi} = \left(2W_1 + 2W_2\lambda^2\right)\left(\lambda - \frac{1}{\lambda^5}\right)$		$T = \left(\frac{2\pi bt}{n}\right)\sigma_{e-bi}$
λ	σ_{e-bi}, lb/in^2	T, lb
1.00	0.0000	0.0000
1.25	23.8743	0.6392
1.50	36.6981	0.9826
1.75	47.1674	1.2629
2.00	57.4875	1.5392
2.50	68.4198	1.8319
2.25	80.3197	2.1505
2.50	93.4073	2.5009
3.00	107.8519	2.8877

* Pre-cycled dimensions: b = 5 in., t = 0.03 in.

Comparing table 2 (pre-tests) and table 10 (post-tests), one notices that the theoretical pulling string tension T at $\lambda = 3$ calculated using the biaxial material constants (W_1 = 11.88, W_2 = 0.68) lb/in^2 is only 48 percent of the value of T calculated using the uniaxial material constants $(W_1 = 7.5,\ W_2 = 2.0)$ lb/in^2.

Figure 35 shows the measured pulling-string tensile forces T required to pull a stress-cycled circular specimen (b = 5.5 in., t = 0.0248 in.) of the silicon rubber to desired radial extension ratios λ. The theoretical T-curve shown in figure 35 is based on the averaged equal-biaxial material constants (W_1 = 11.88, W_2 = 0.68) lb/in^2 (table 8). Note that the theoretical T-curve compares fairly well with the experimental T-curves.

Transverse Uniaxial Tests

For exploration purposes, from the longitudinally tested uniaxial specimen (fig. 36), a small uniaxial test sample was cut off, and stretched in a transverse direction to compare the stress-stretch curves associated with the two orthogonal directions. Figure 37 shows a family of transverse stress-stretch curves associated with different stress cycling. Note that after the first stress cycling, the subsequent stress-stretch curves bend concave upwardly at large stretching.

Figure 38 shows that the stress-stretch curves associated with the two orthogonal directions are relatively close in the low stretch region up to $\lambda = 4.5$ beyond which the two curves diverge, indicating stretch-induced material property change.

As mentioned earlier, the molecular-chains crystallizations occur significantly more in the uniaxial stress field than in the biaxial stress field because the molecular chains can easily form a regular lattice in the case of uniaxial stretching where two degrees of freedom are available for lateral contractions. Thus, the uniaxial-stretching induced material property change explains why the values of $\{W_1, W_2\}$ determined from the uniaxial stress field are marked different from the values of $\{W_1, W_2\}$ determined from the equal-biaxial tests (see table 8). Therefore, the traditional way of simply using the material constants $\{W_1, W_2\}$ determined from the uniaxial tensile tests to establish the theoretical constitutive equation (2) is unsound. The values of $\{W_1, W_2\}$ must also be determined from the equal-biaxial stress field. Keep in mind that in practical applications, hyperelastic membranes are usually under biaxial stress fields and not under a pure uniaxial stress field as in the case of stretching a rubber ring.

Concluding Remarks

Uniaxial, equal-biaxial, and strip-biaxial tensile tests were conducted to obtain stress-stretch data for determining the material constants (strain-energy gradients) for hyperelastic silicon rubber (a potential candidate elastomer for aerospace applications). The resulting stress-stretch data were then re-plotted as stress-difference plots, modified stress-difference plots, and energy plots from which the material constants were graphically determined by using the trendline method. The material constants were also determined from MSC-MARC® direct curve-fitting of the stress-stretch data. Based on the experimentally determined material constants, the theoretical constitutive equations were established for the silicon rubber. Some key findings are listed below:

1. The material constants $\{W_1, W_2\}$ determined from uniaxial, equal-biaxial, and strip-biaxial stress fields are quite different, indicating that material behavior is stress-field dependent.
2. The constitutive equation established based on material constants determined from uniaxial tensile tests cannot be used for biaxial stress fields because of stretch induced molecular-chains crystallizations, which occur significantly more in the uniaxial stress field than in the biaxial stress field.
3. The longitudinally stretched uniaxial test specimen was also stretched in a lateral direction. The stress-stretch curves in the two orthogonal directions are substantially different at high extensions, indicating stretch-induced material anisotropy.

4. The material constants determined from equal-biaxial energy plots and the MSC-MARC® combined (uniaxial and biaxial) curve fitting method was found to be very close and could be considered as universal material constants for establishing the universal constitutive equation for describing the material behavior of silicone rubber in both uniaxial and biaxial stress fields.

5. The energy plots for uniaxial and strip-biaxial stress fields give values of W_1 comparable to the value of W_1 determined from the equal-biaxial stress field, but giving unrealistic values of W_2. Thus, the energy plot should be used only for the equal-biaxial stress field.

6. Using the linear trendline method on the stress-difference plots, modified stress-difference plots, and energy plots, one can visualize how the values of $\{W_1, W_2\}$ are graphically displayed.

Figures

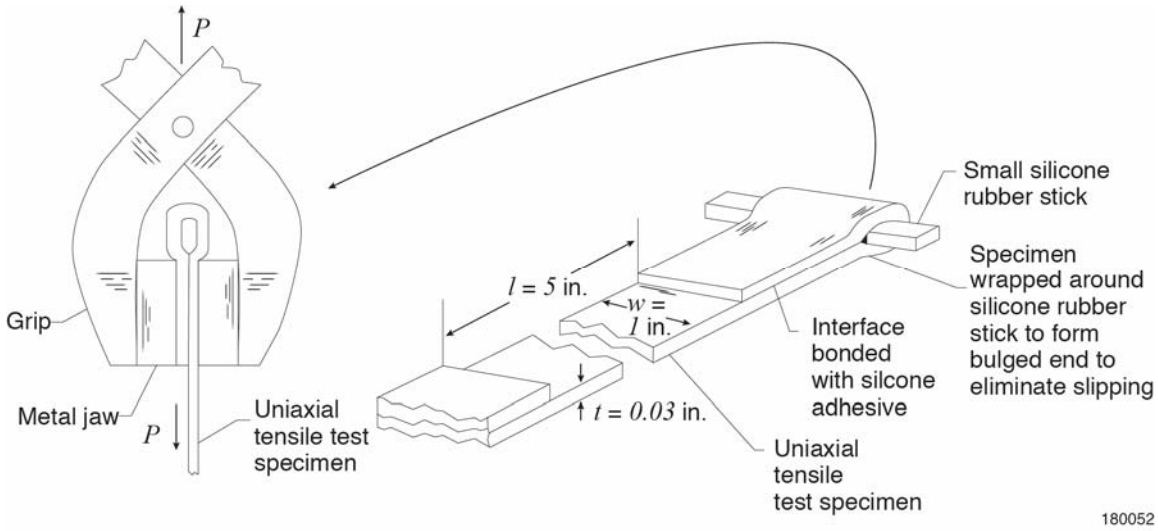

Figure 1. Uniaxial tensile tests: The NASA-AFRC-FLL method for gripping the uniaxial tensile test specimen of hyperelastic material by using wrapping-around bulged ends to stop the specimen from slipping from the self-tightening scissor grip clamp at large extensions.

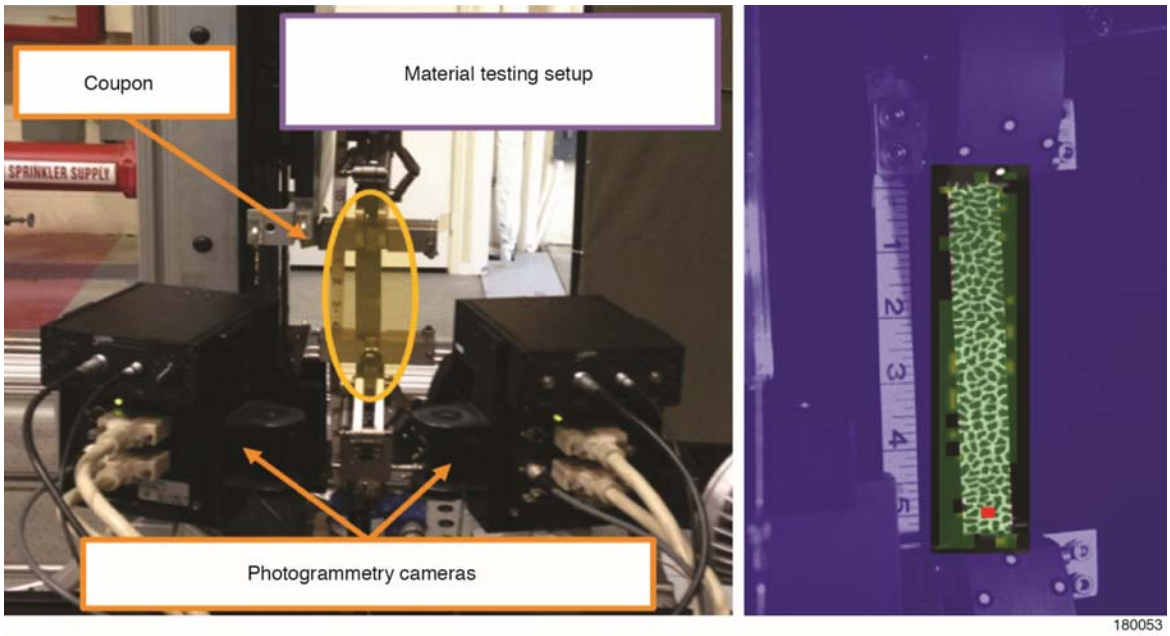

Figure 2. Uniaxial tensile test setup: extension ratio λ is measured by a measuring tape or by photogrammetry cameras recording the displacements of transverse marking lines or dotted grid points on the specimen surface; over-all view of the uniaxial tensile test system (left); and retracted specimen from $\lambda = 8$ (right).

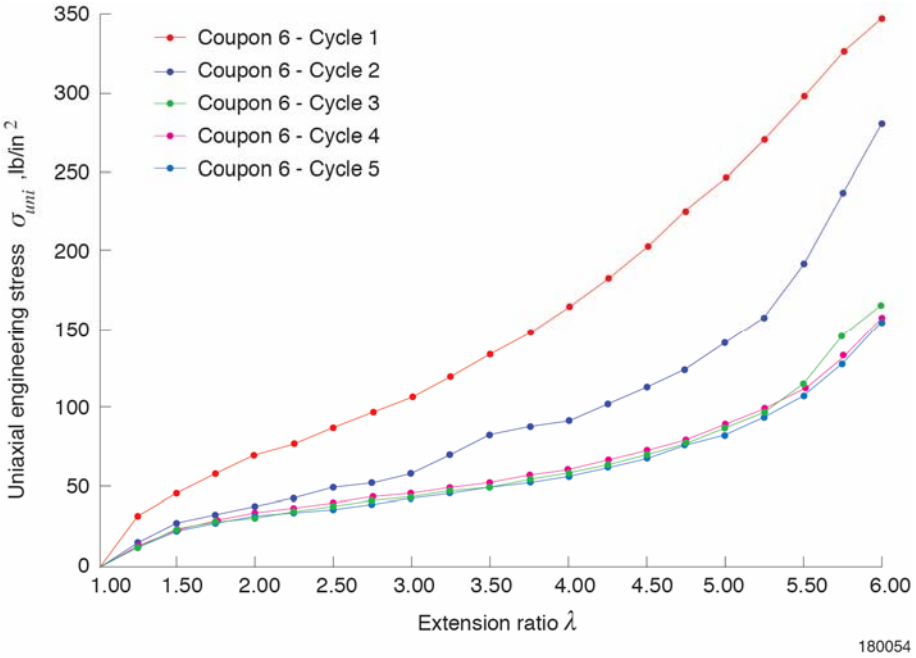

Figure 3. The uniaxial stress-stretch curve of silicone rubber changes with the number of stress cyclings; marked variation shows a high degree of material softening after stress cyclings; and the stress-stretch curve reached steady state at the fifth stress cycling.

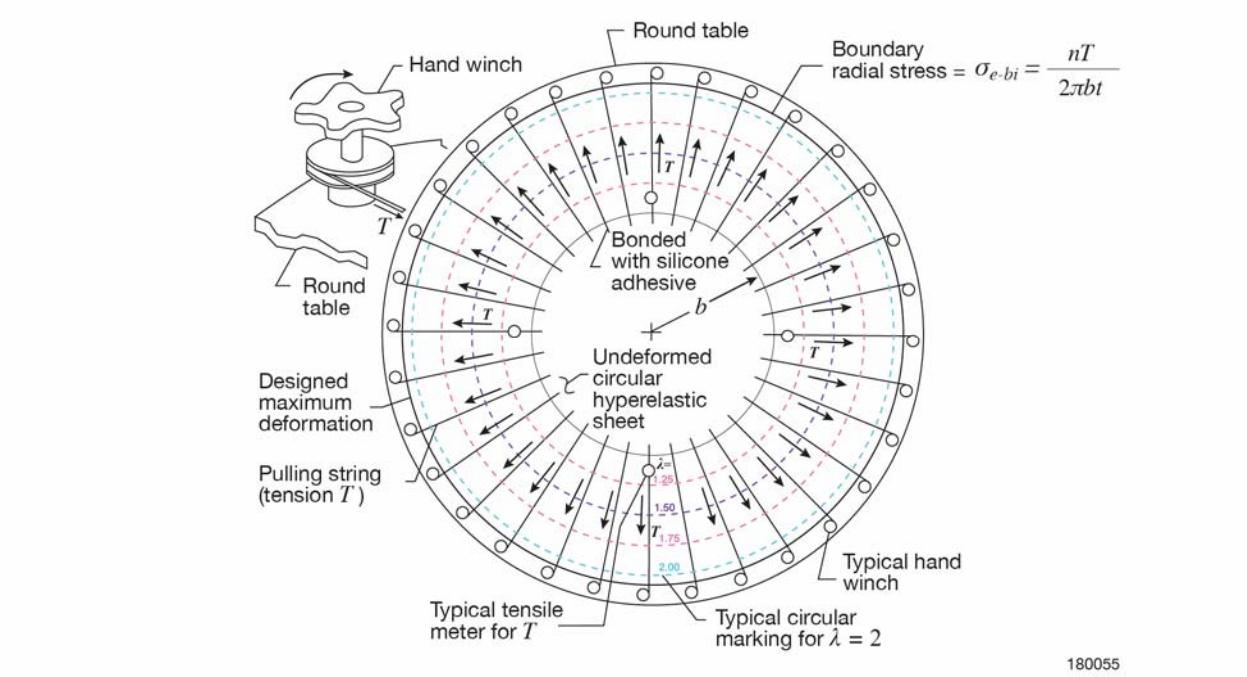

Figure 4(a). Design concept.

Figure 4(b). Actual top view.

Figure 4. Design concept and actual top view of the low-cost, manually operated five-foot-diameter radial-biaxial test round table for obtaining equal-biaxial tensile stress-stretch data using n = 32 radial pulling strings.

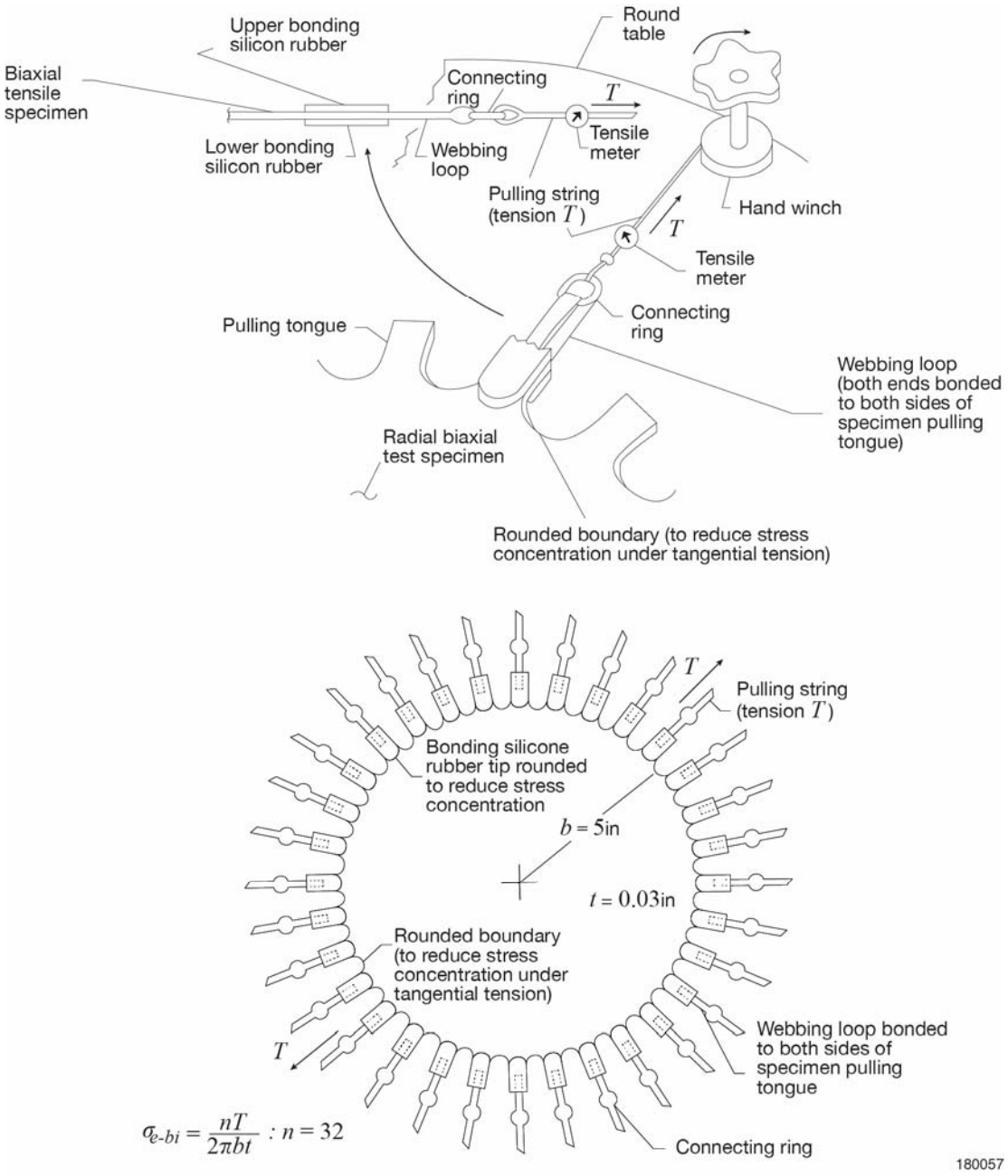

Figure 5. Gear-shaped boundary (Type 1) FLL radial-biaxial tensile test specimen (radius b = 5 in., thickness t = 0.03 in.); through connecting rings, n = 32 pulling strings are connected to webbing loops whose two ends are bonded respectively to the specimen periphery upper and lower surfaces.

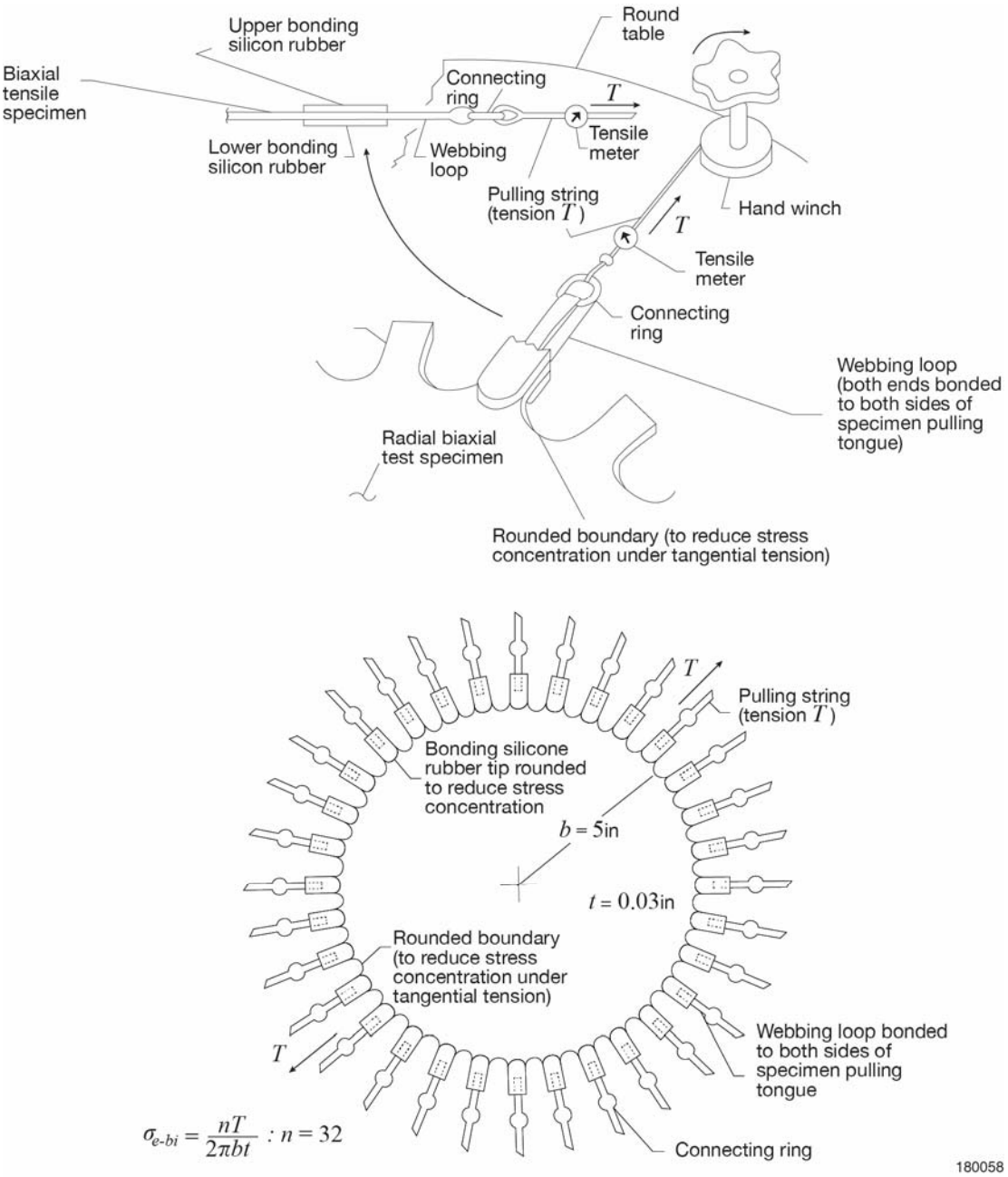

Figure 6. Smooth boundary (Type 2) FLL radial-biaxial tensile test specimen (radius b = 5 in., thickness t = 0.03 in.); through connecting rings, n = 32 pulling strings are connected to webbing loops whose two ends are bonded respectively to the specimen periphery upper and lower surfaces.

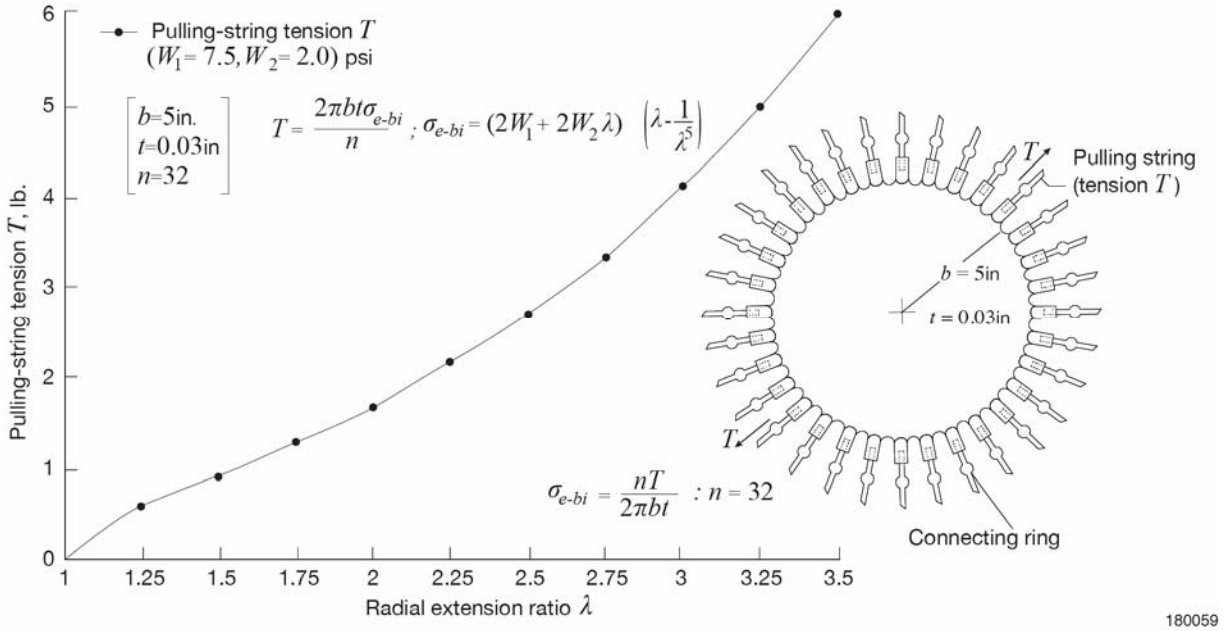

Figure 7. Pre-test estimated pulling-string tensile force T required to pull a circular sheet (b = 5 in., t = 0.03 in.) of silicon rubber material [$(W_1 = 7.5, W_2 = 2.0)$lb/in^2] to the desired radial extension ratio λ using n = 32 equally spaced boundary pulling strings.

Figure 8. Over-all view of the radial-biaxial tensile test round table constructed at the NASA AFRC-FLL for radial-biaxial tensile tests of hyperelastic materials [under NASA New Technology Reporting protection (NTR) DRC-017-007].

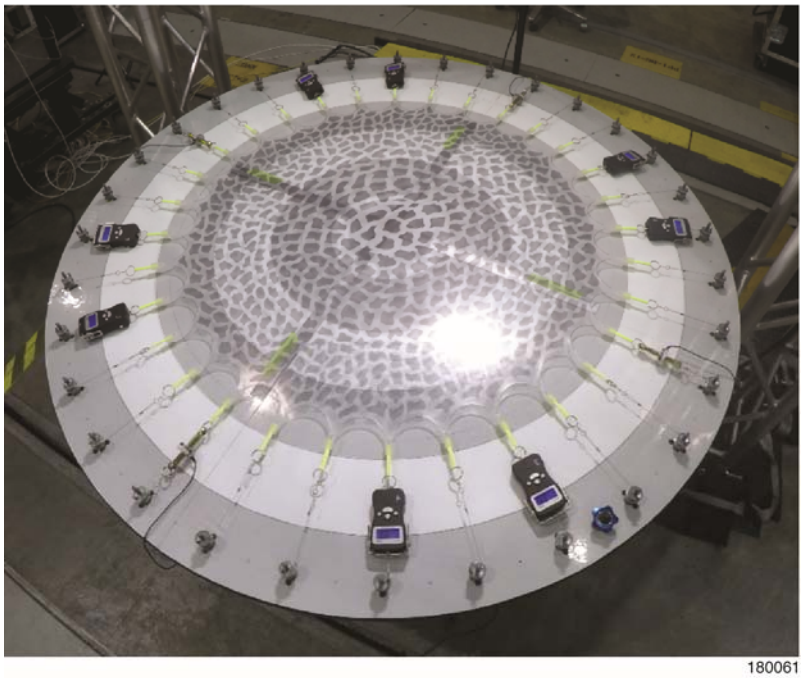

180061

Figure 9. Close-up view of the AFRC-FLL five-foot-diameter radial-biaxial tensile test round table; the specimen is radially pulled by the $n = 32$ miniature hand winch anchored near the edge of the round table; the pulling string tensile forces are measured by using miniature tensile meters; and concentric circles are drawn on the round table to indicate different radial extension ratios for the deformed specimen boundary to match.

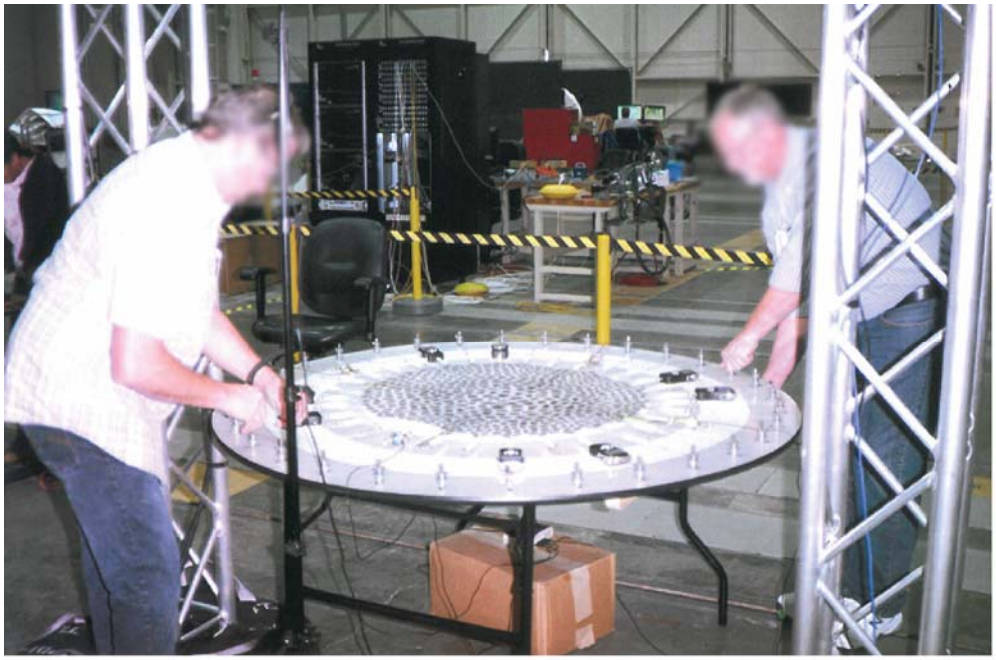

180062

Figure 10. Radial stretching of the specimen is accomplished by two persons by step-wisely turning each pair of manual winches at diametrically opposite sides of the radial-biaxial tensile test round table.

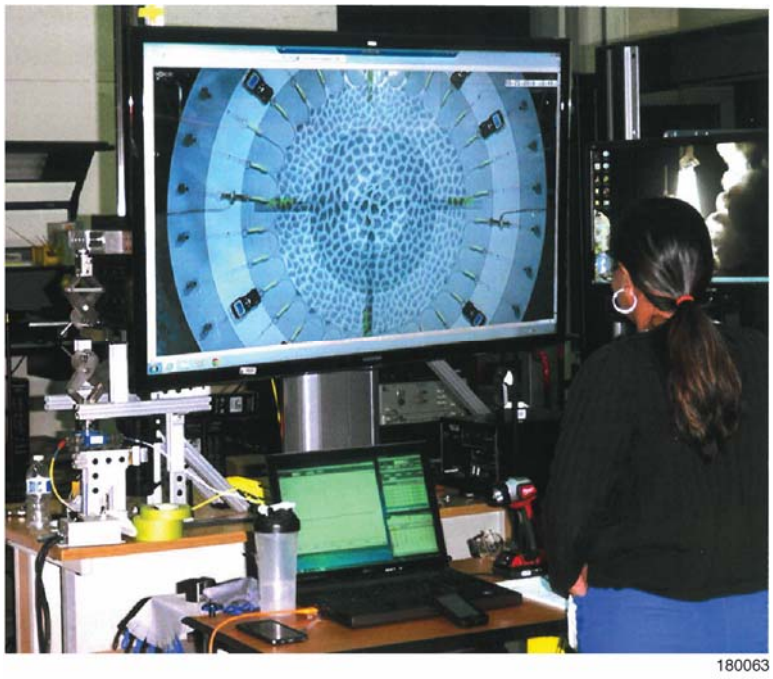

Figure 11. Screen image of the stretched specimen generated from the overhead camera was used for fine-tuning the pulling-string tension so as to bring the stretched specimen boundary to match a particular concentric circle drawn on the radial-biaxial tester round table, giving the desired radial (= tangential) extension ratio λ_∞.

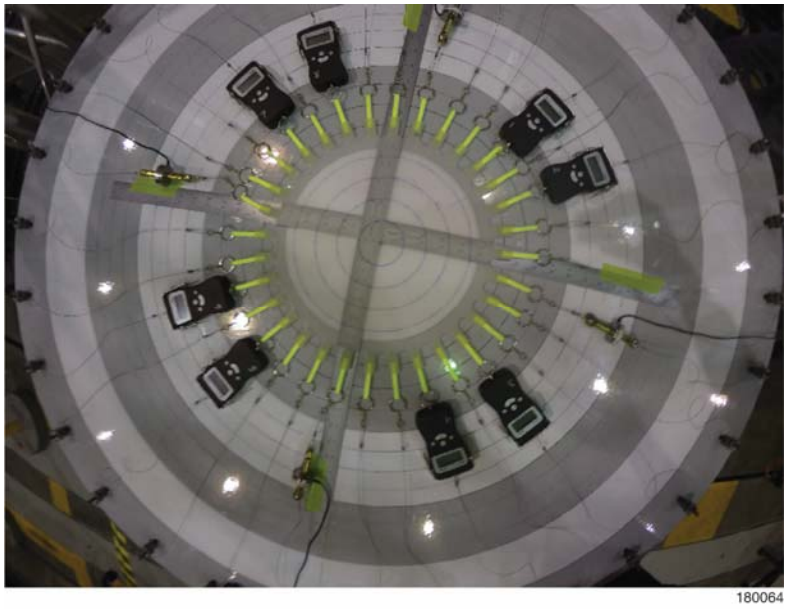

Figure 12(a). Undeformed, $\lambda = 1$.

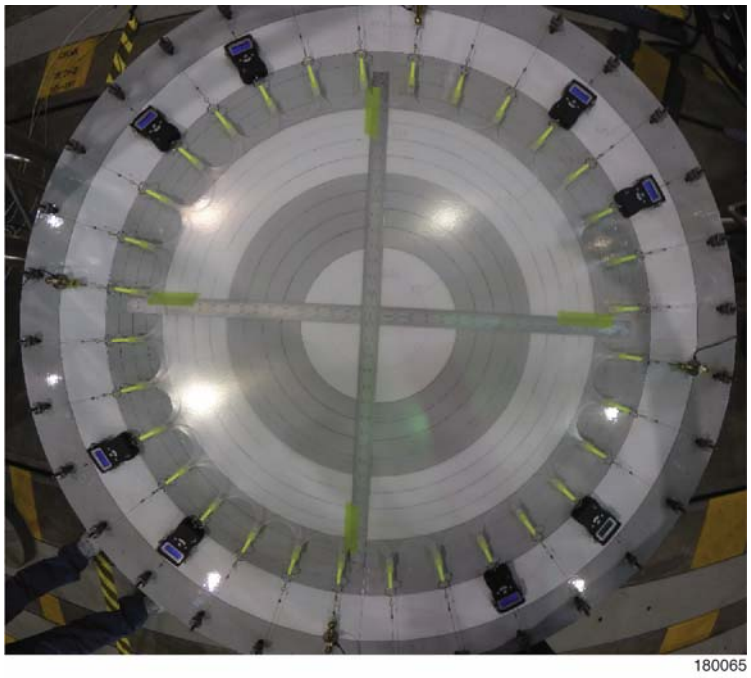

Figure 12(b). Deformed, $\lambda = 3$.

Figure 12. Radial-biaxial tensile test specimen of silicone rubber with gear-shaped boundary before and after stretching (undeformed dimensions; b = 5 in., t = 0.03 in.).

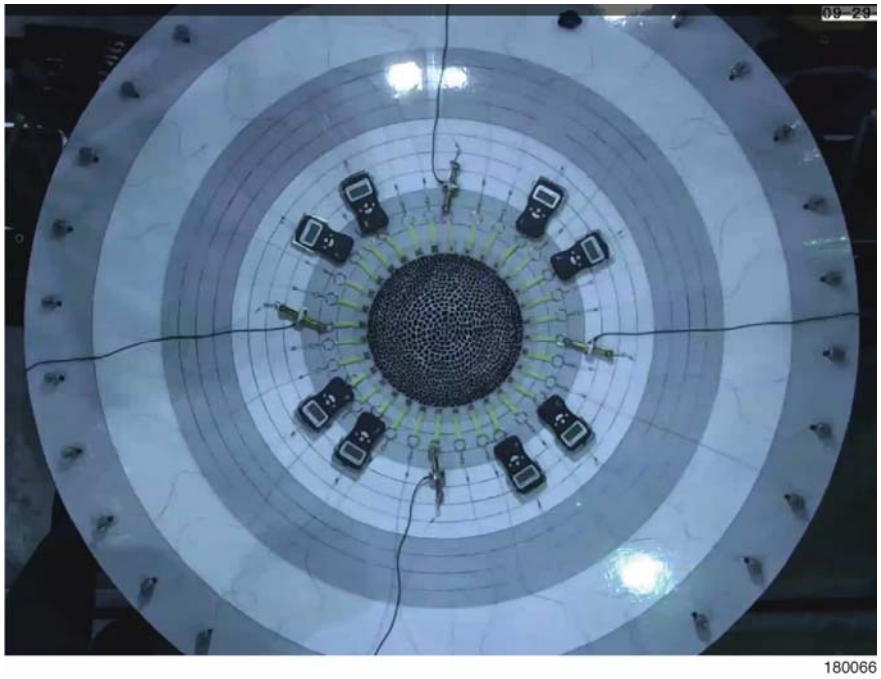

Figure 13(a). Undeformed, $\lambda = 1$.

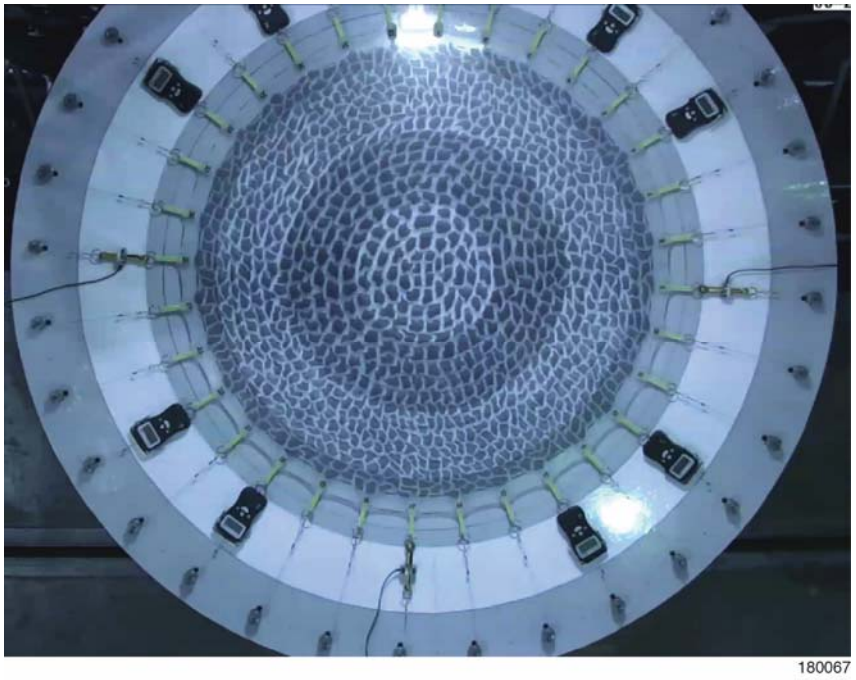

Figure 13(b). Deformed, $\lambda = 3.25$.

Figure 13. Radial-biaxial tensile test specimen of silicone rubber with a smooth boundary before and after stretching; undeformed dimensions (b = 5 in., t = 0.03 in.).

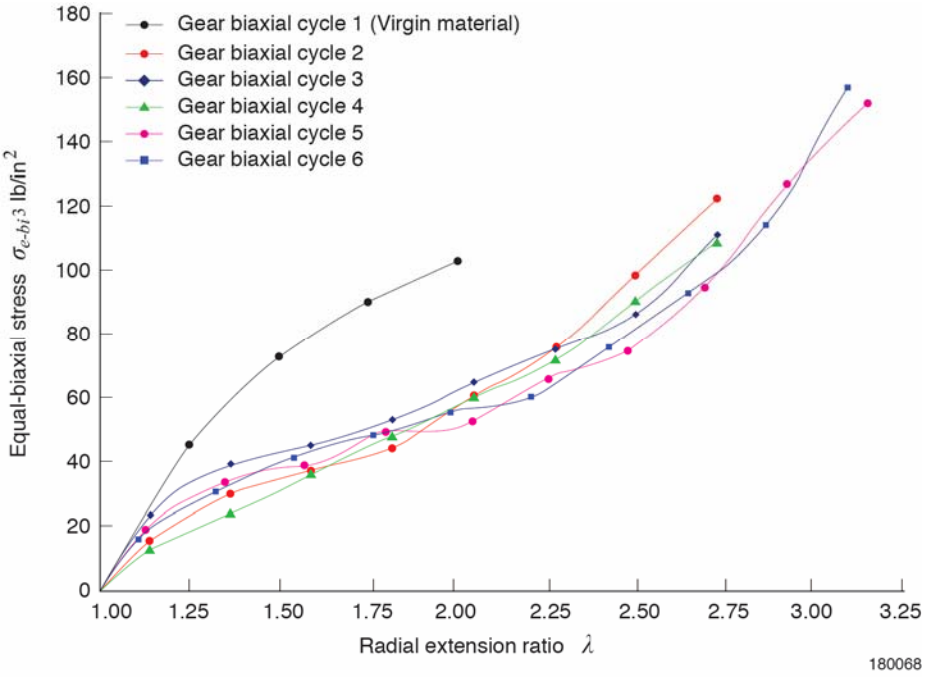

Figure 14(a). Gear-shaped boundary.

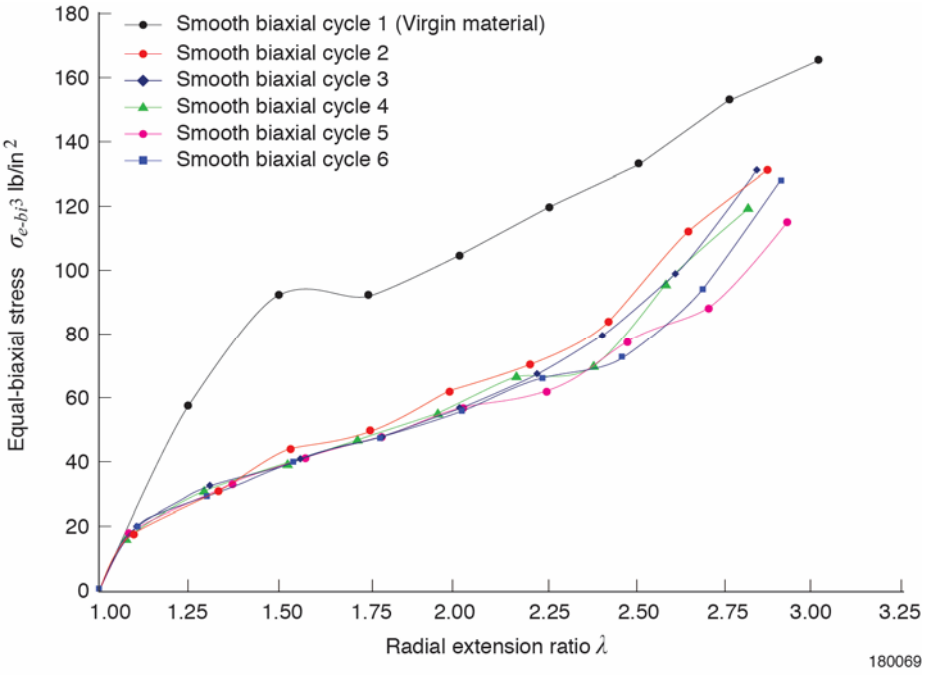

Figure 14(b). Smooth boundary.

Figure 14. Equal-biaxial stress-stretch curves at different stress-cyclings. After the first stress cycling of a virgin silicone rubber specimen, high degree of material softening was practically eliminated, causing the rest of the stress-stretch curves to form a narrow band.

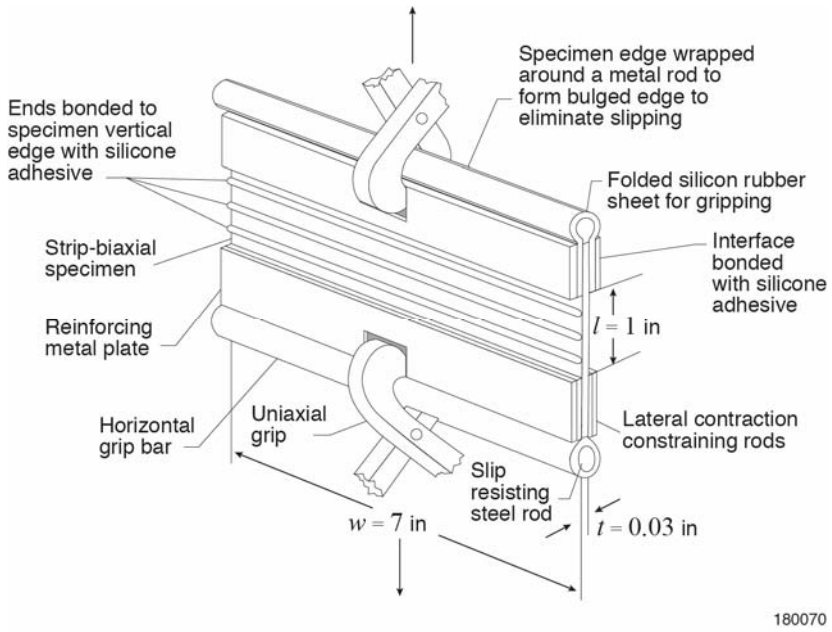

Figure 15. Strip-biaxial (laterally constrained uniaxial) tensile test setups to obtain stress-stretch data for determinations of material constants summation $(W_1 + W_2) = \mu/2$. Metal plates are bonded to folded gripping silicon rubber sheets for maintaining grip on straight edges. Specimen dimensions: length l = 1 in., width w = 7 in., and thickness t = 0.03 in.

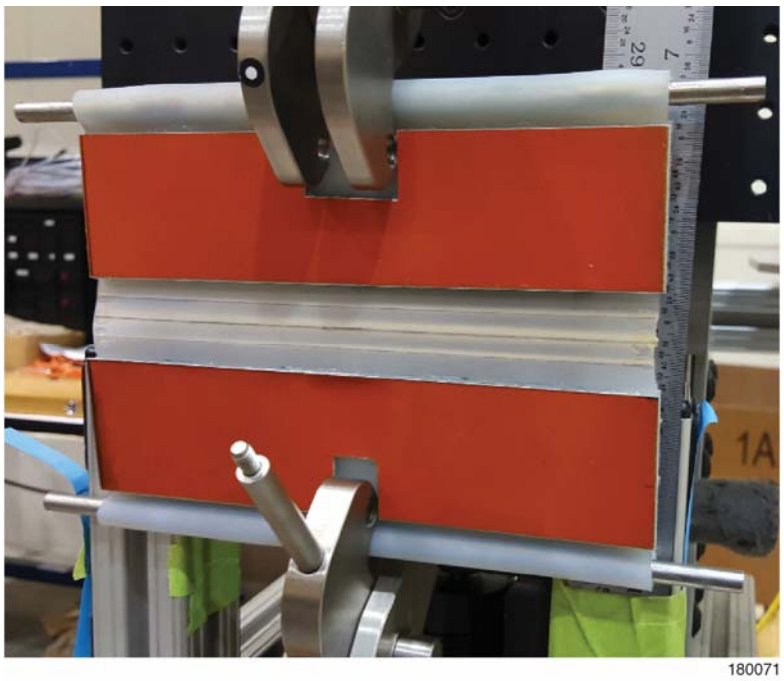

Figure 16(a). Undeformed, $\lambda = 1$.

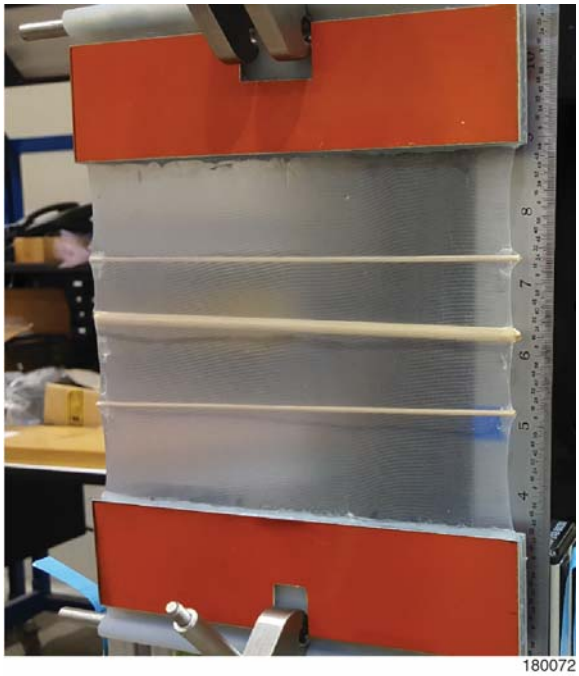

Figure 16(b). Stretched to $\lambda = 4.7$.

Figure 16. Strip-biaxial tensile test specimen (silicone rubber) before and after deformation (undeformed dimensions: l = 1 in., w = 7 in., t = 0.03 in.). Specimen vertical edge contraction is constrained by using constraining rods with their ends bonded to the specimen free edges.

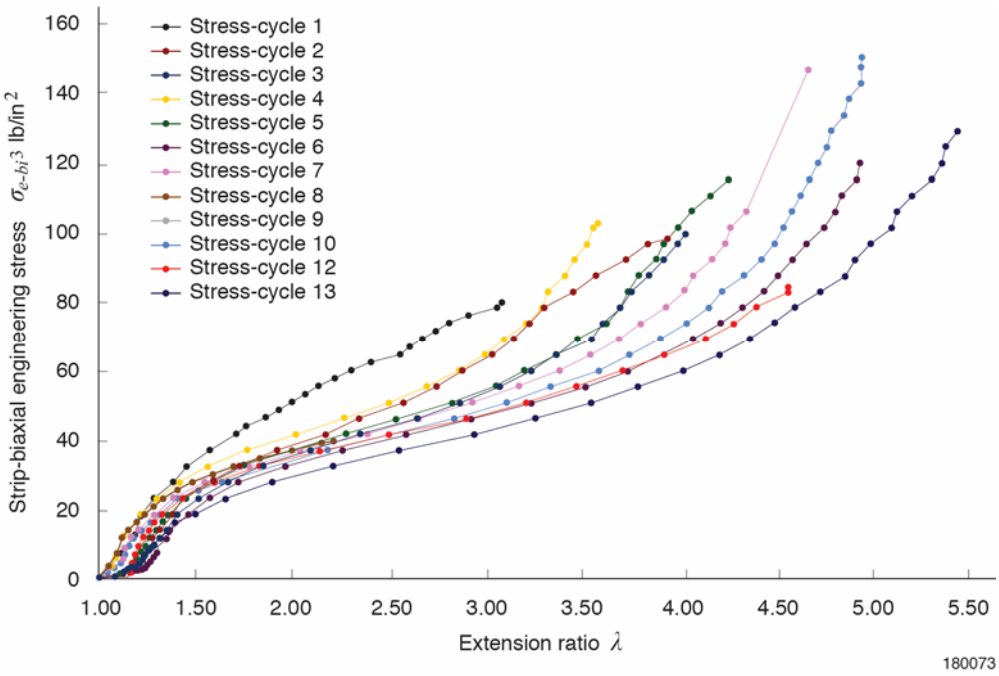

Figure 17. Strip-biaxial stress-stretch curves of silicone rubber at different stress-cyclings, showing a high degree of material softening after stress cyclings.

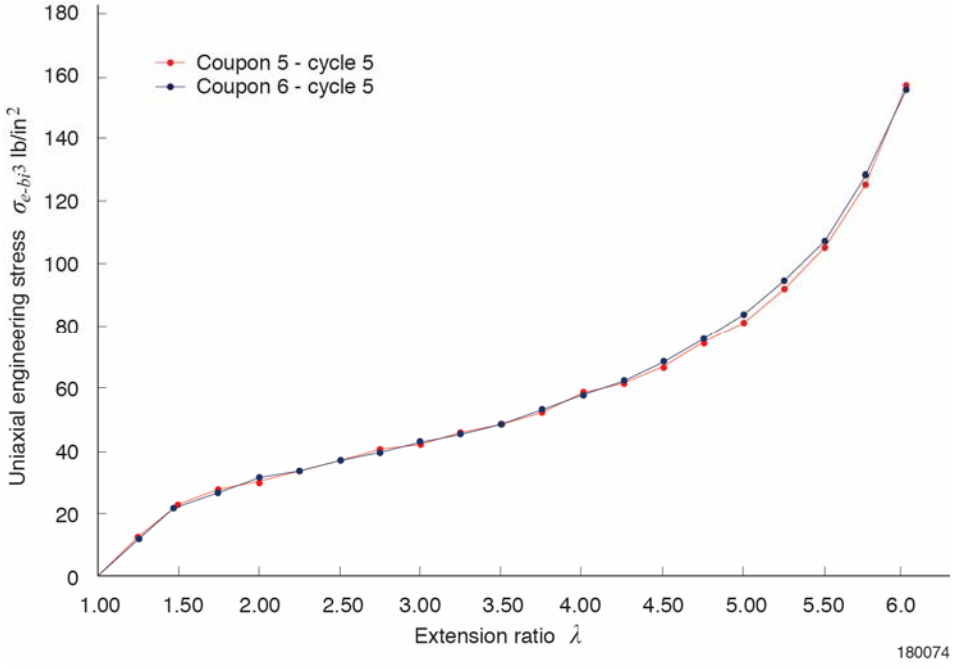

Figure 18. Uniaxial stress-strain data of silicone rubber used to determine the material constants $\{W_1, W_2\}$.

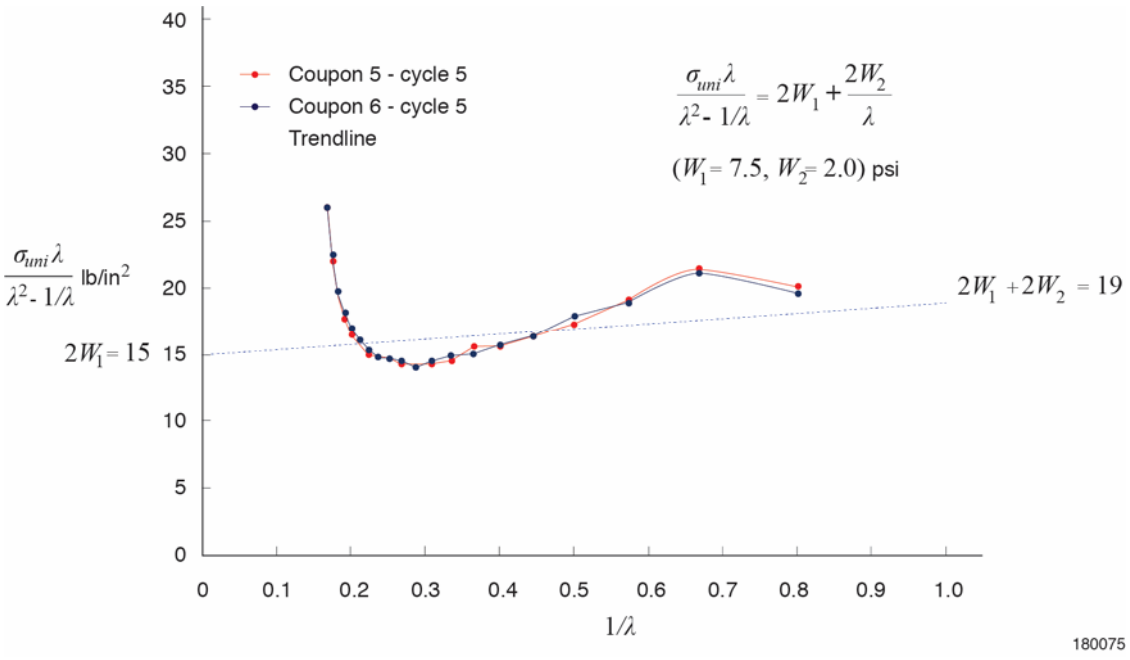

Figure 19. Uniaxial Type-1 plots [stress-difference plot, eq. (3)] for determining material constants $\{W_1, W_2\}$ for silicone rubber using the linear trendline method $\{W_1 = 7.5, W_2 = 2.0\}$ lb/in^2.

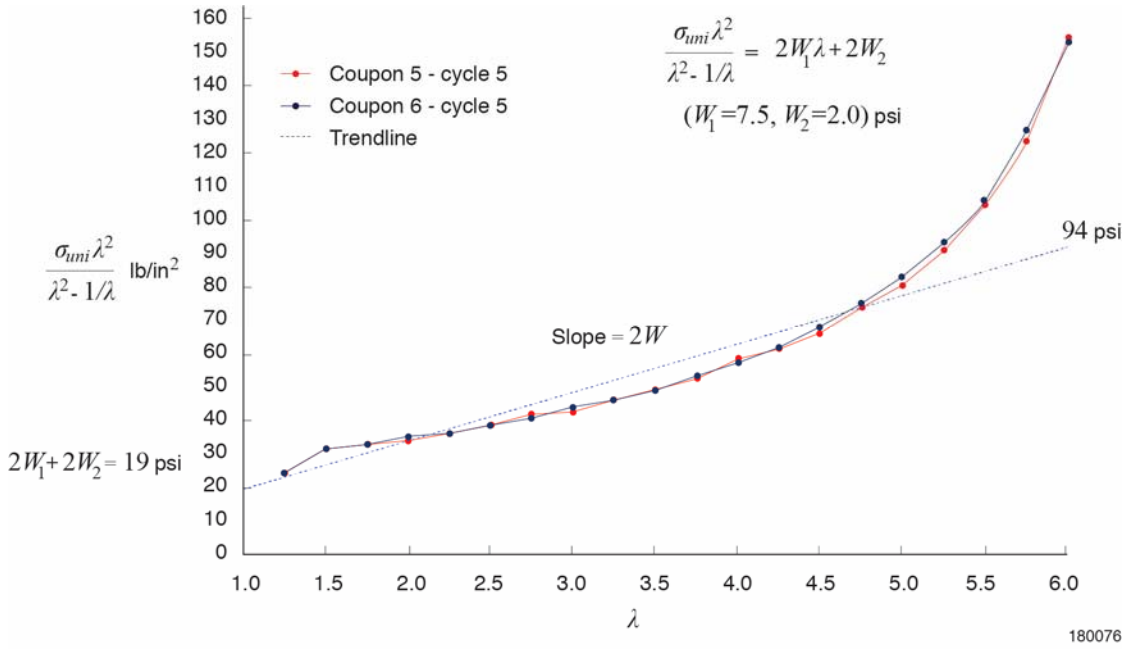

Figure 20. Uniaxial Type-2 plots [modified stress difference plot, eq. (4)] for determining material constants $\{W_1, W_2\}$ for silicone rubber using the linear trendline method $\{W_1 = 7.5, W_2 = 2.0\}$ lb/in^2.

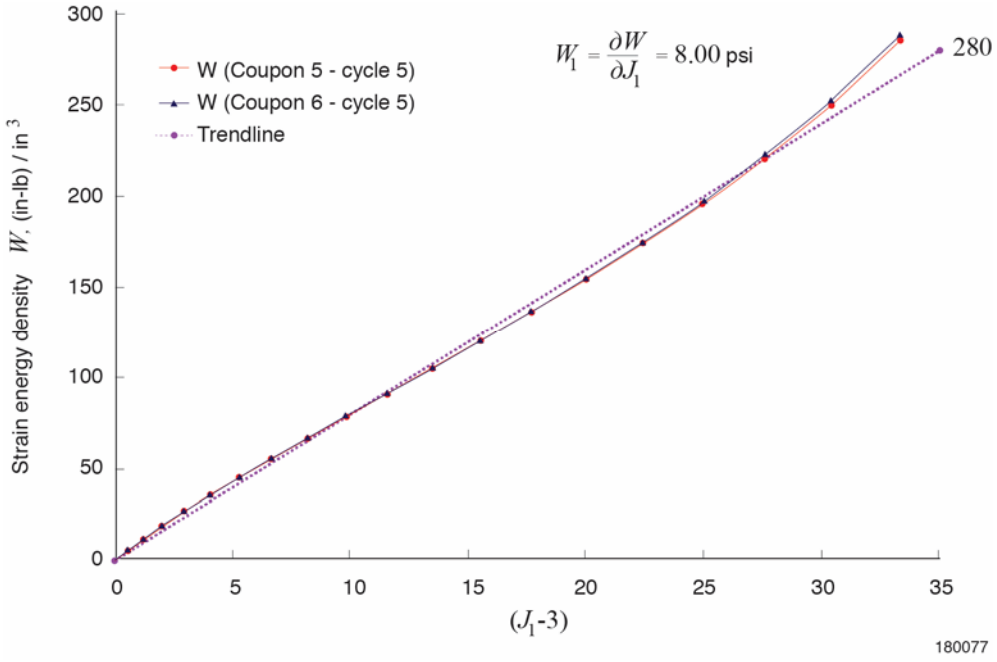

Figure 21. Plots of uniaxial strain energy density data of W [eq. (13)] as functions of $(J_1 - 3)$ for determining material constant W_1 for silicone rubber ($W_1 = 8.00$ lb/in^2).

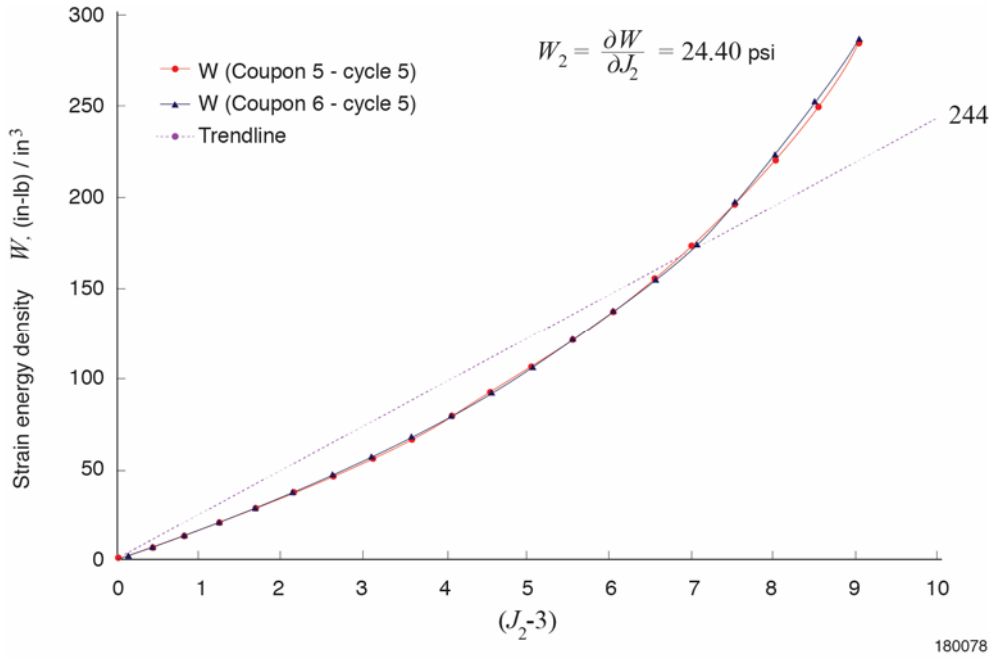

Figure 22. Plots of uniaxial strain energy density data of W [eq. (13)] as functions of $(J_2 - 3)$ for determining material constant W_2 for silicone rubber ($W_2 = 24.40$ lb/in^2).

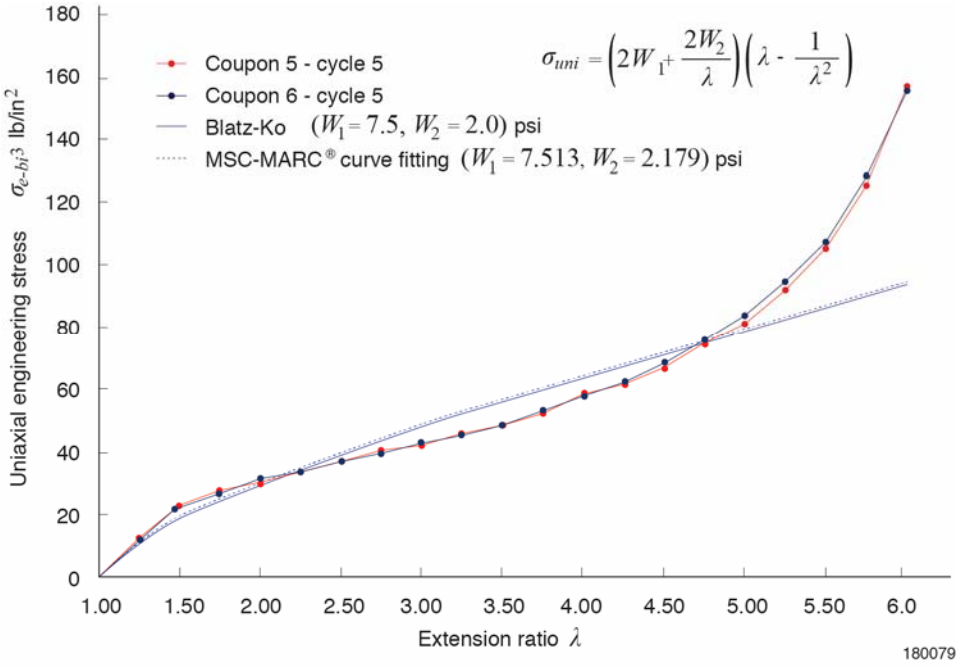

Figure 23. Comparisons of theoretical and experimental uniaxial stress-strain curves for silicone rubber: the trendline method (W_1 = 7.5 lb/in^2, W_2 = 2.0 lb/in^2); and the MSC-MARC® curve-fitting method (W_1 = 7.513 lb/in^2, W_2 = 2.179 lb/in^2).

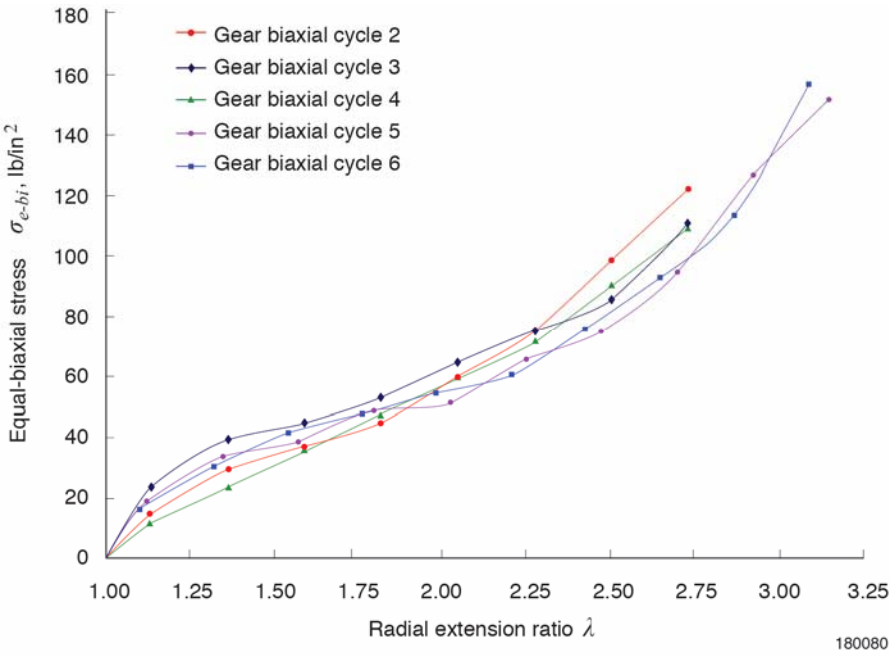

Figure 24(a). Gear-shaped specimen.

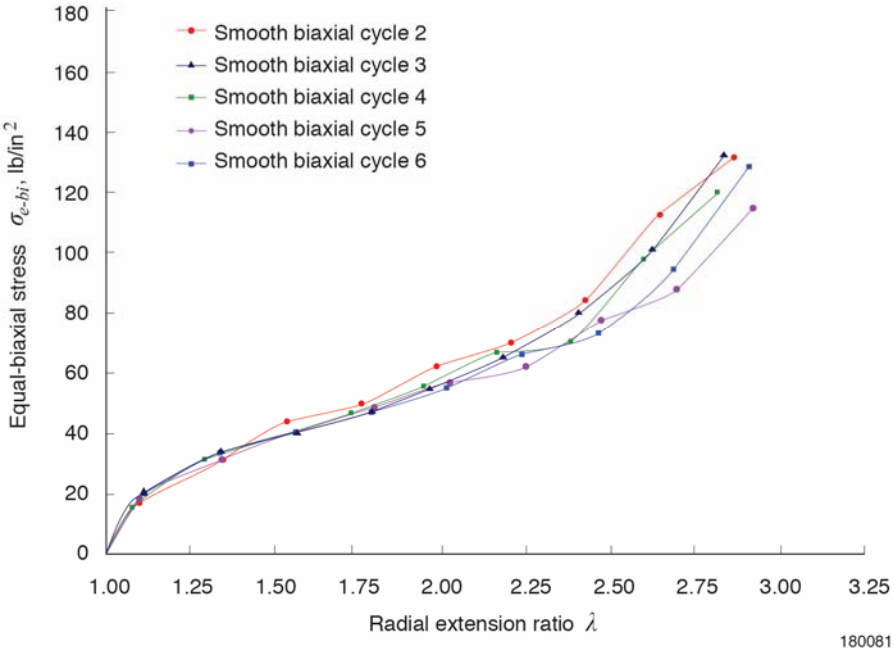

Figure 24(b). Smooth specimen.

Figure 24. Equal-biaxial stress-strain data of silicone rubber used to determine the material constants $\{W_1, W_2\}$.

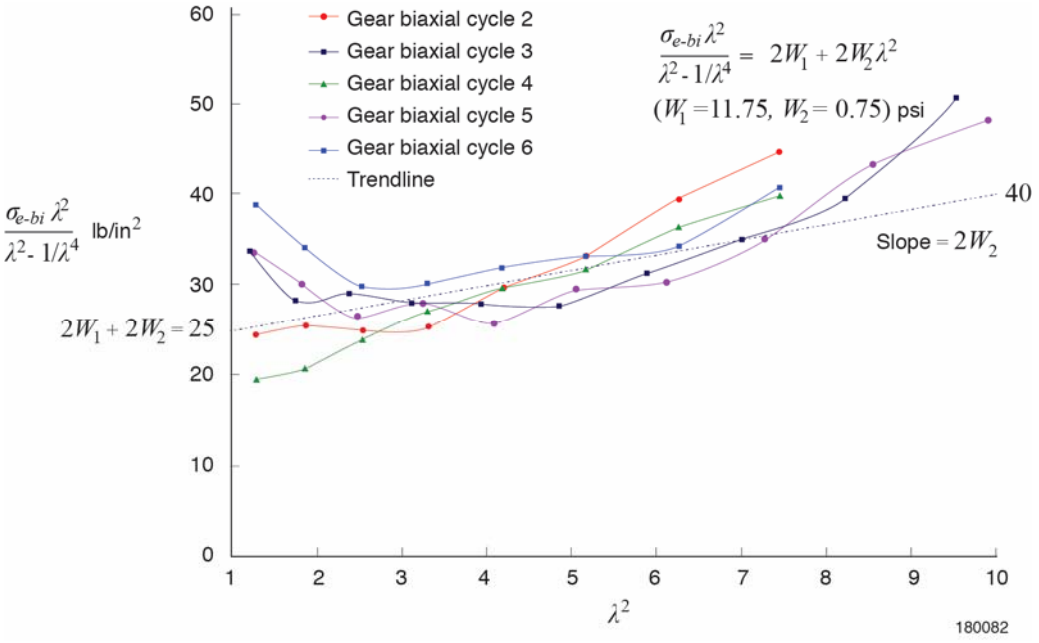

Figure 25(a). Gear-shaped specimen $(W_1 = 11.75,\ W_2 = 0.75)$ lb/in^2.

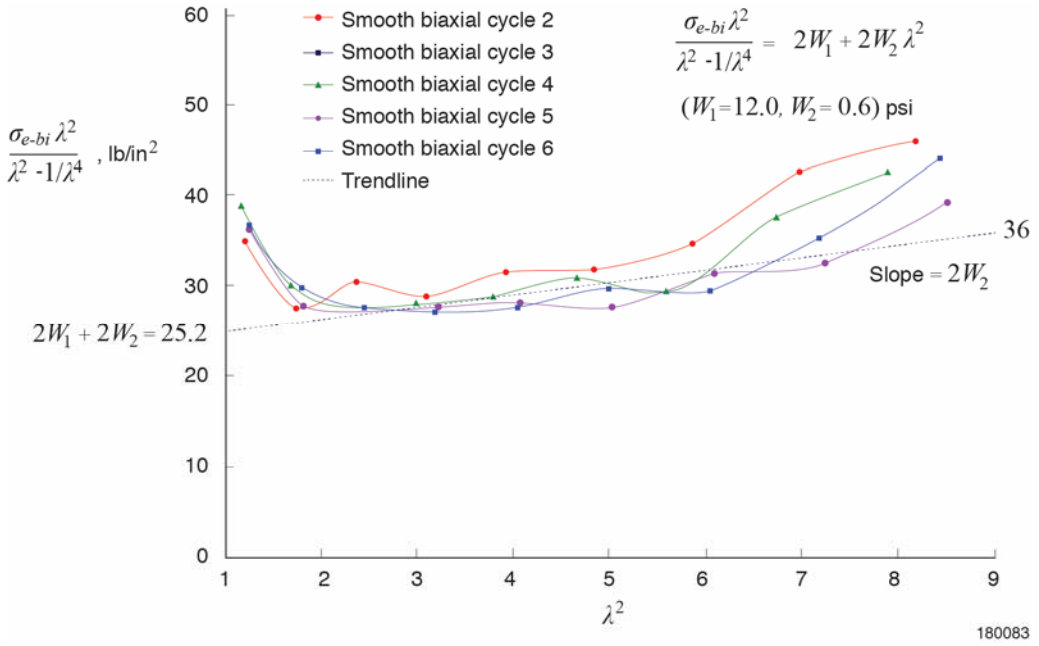

Figure 25(b). Smooth specimen $(W_1 = 12.00,\ W_2 = 0.60)$ lb/in^2.

Figure 25. Equal-biaxial Type-1 plots [stress-difference plots, eq. (3)] for determining material constants $\{W_1, W_2\}$ for silicone rubber using the linear trendline method.

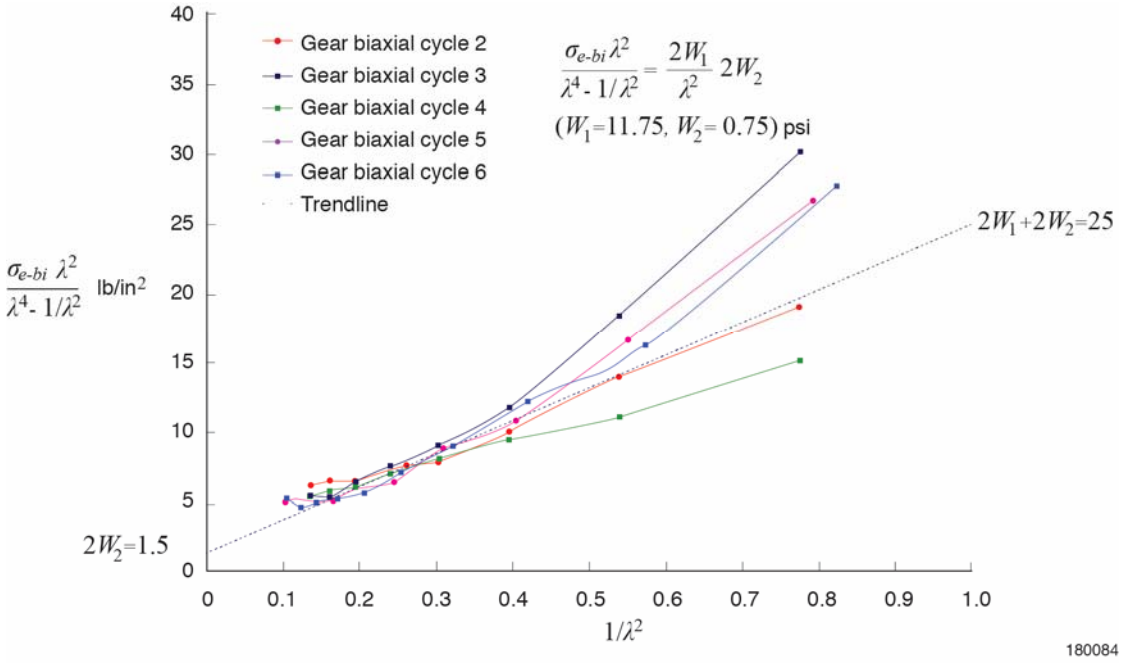

Figure 26(a). Gear-shaped specimen $(W_1 = 11.75,\ W_2 = 0.75)$ lb/in^2.

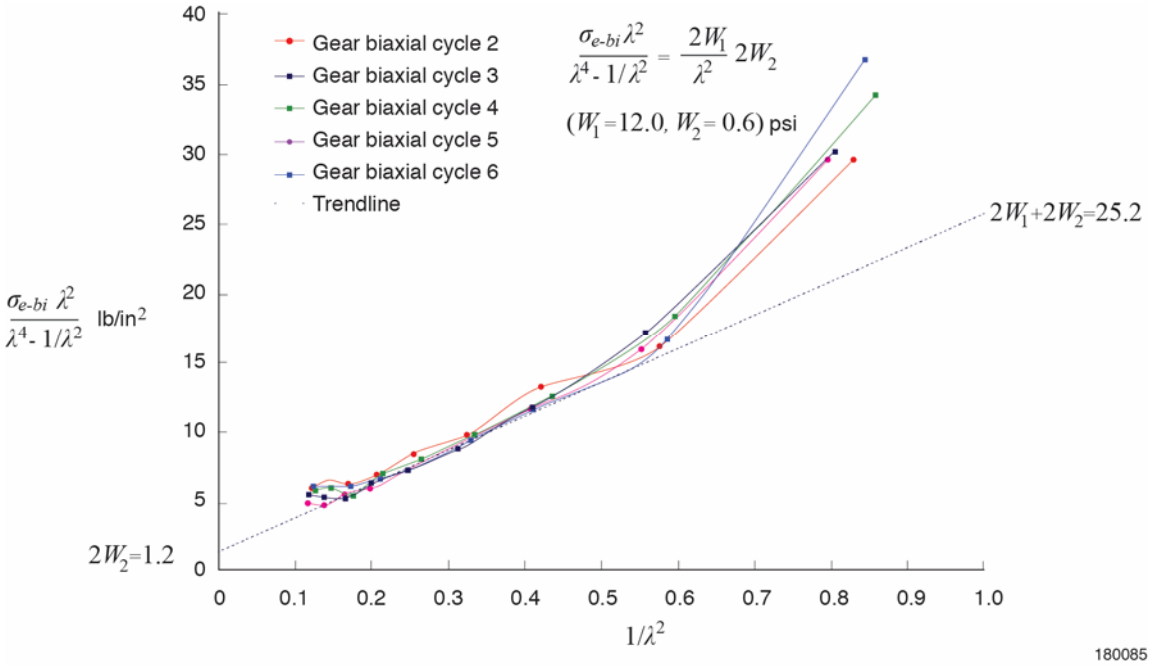

Figure 26(b). Smooth specimen $(W_1 = 12.00,\ W_2 = 0.60)$ lb/in^2.

Figure 26. Equal-biaxial Type-2 plots [stress-difference plots, eq. (4)] for determining material constants $\{W_1, W_2\}$ for silicone rubber using the linear trendline method.

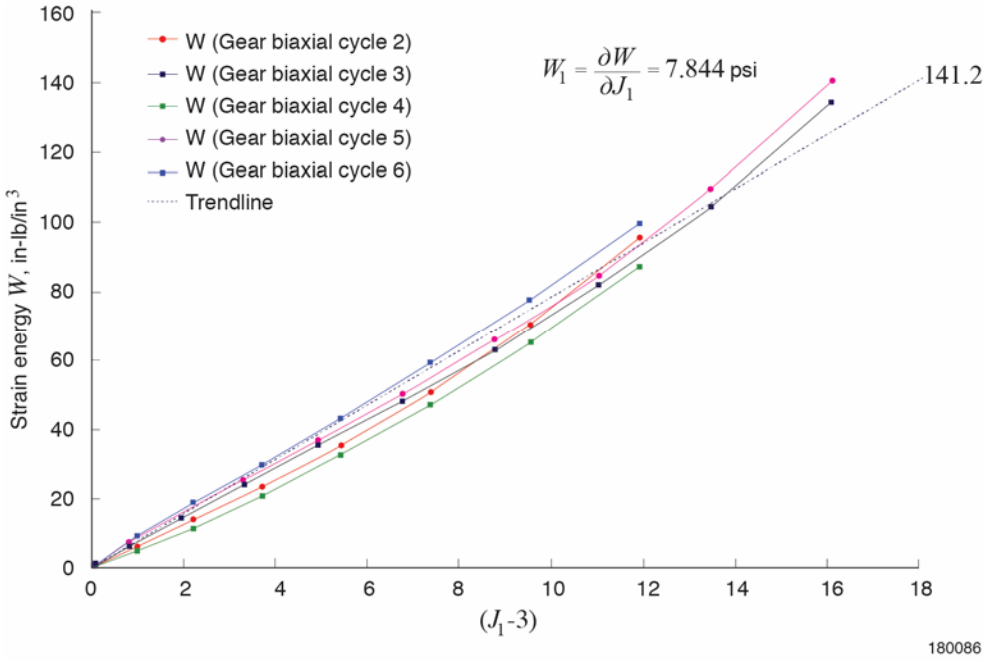

Figure 27(a). Gear-shaped specimen $(W_1 = 7.844$ lb/in$^2)$.

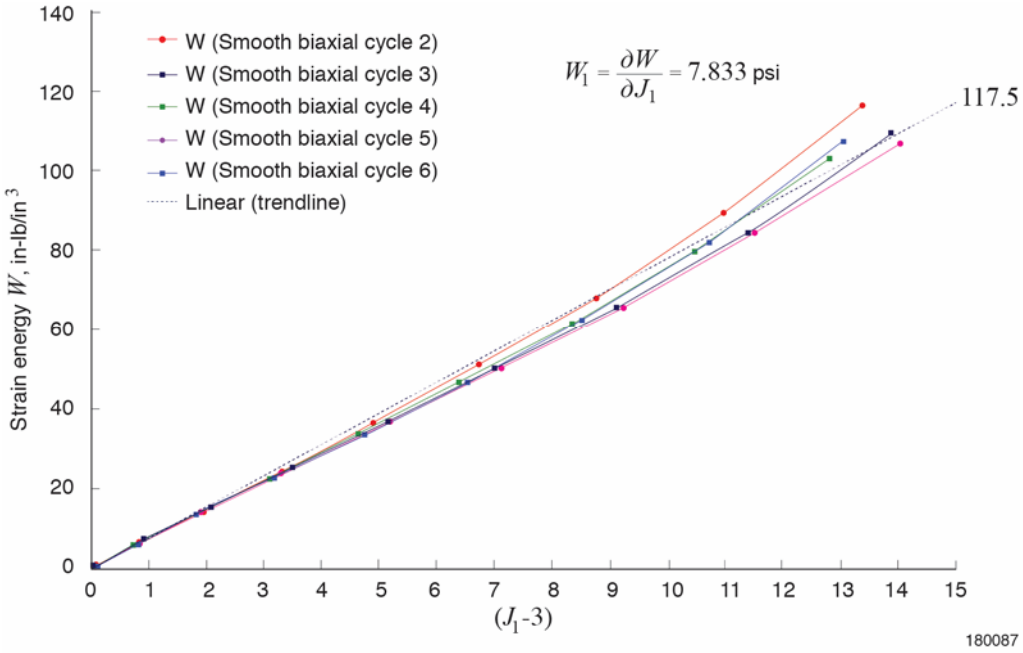

Figure 27(b). Smooth specimen $(W_1 = 7.833$ lb/in$^2)$.

Figure 27. Plots of equal-biaxial strain energy density data of W [eq. (13)] as functions of $(J_1 - 3)$ for determining material constant W_1 for silicone rubber.

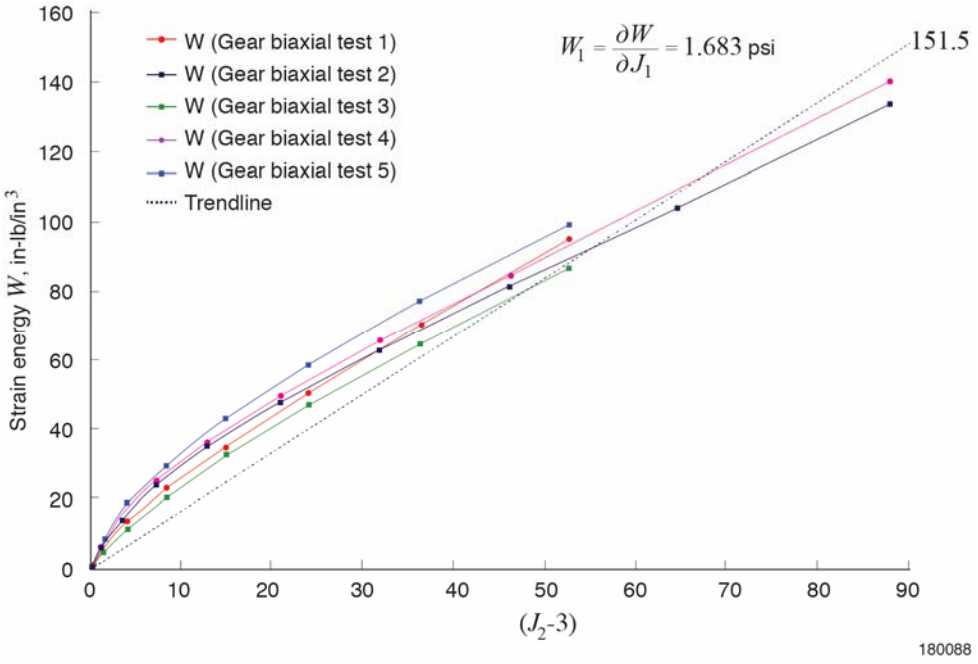

Figure 28(a). Gear-shaped specimen $(W_2 = 1.683$ lb/in$^2)$.

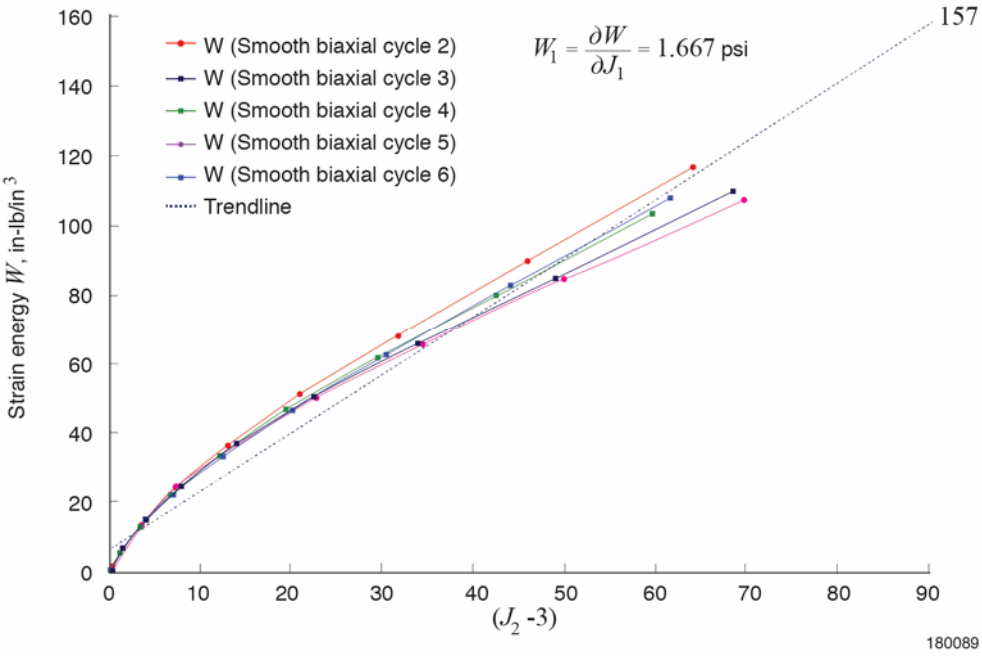

Figure 28(b). Smooth specimen $(W_2 = 1.667$ lb/in$^2)$.

Figure 28. Plots of equal-biaxial strain energy density data of W [eq. (13)] as functions of $(J_2 - 3)$ for determining material constant W_2 for silicone rubber.

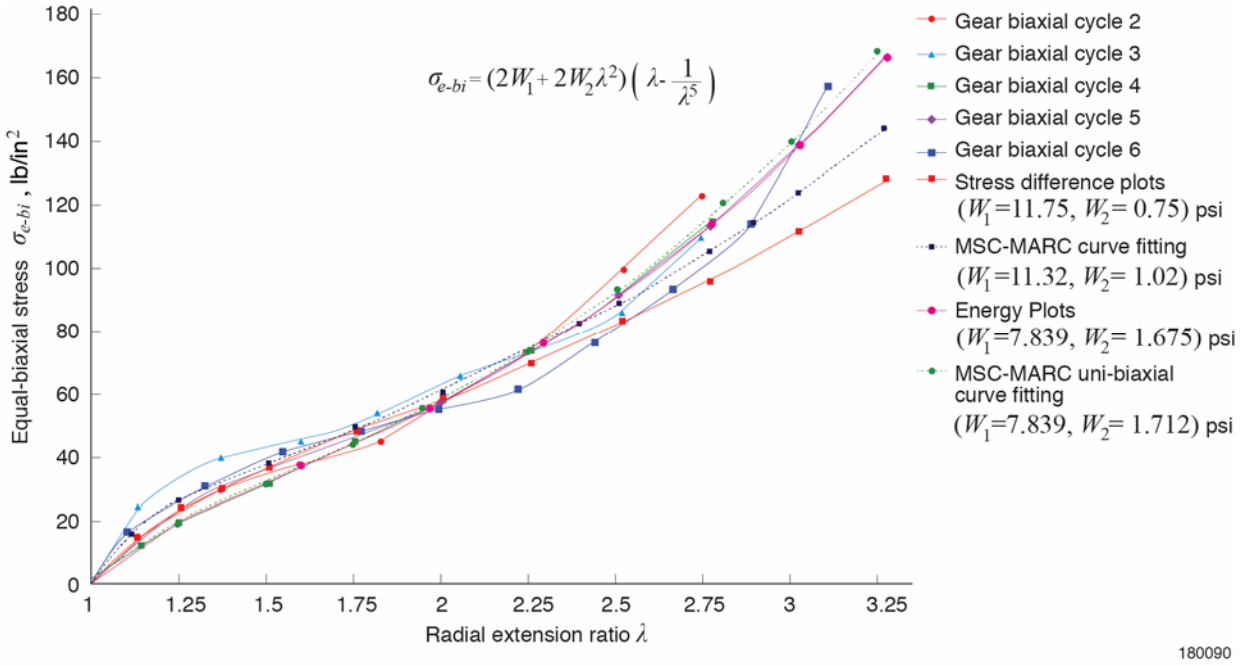

Figure 29(a). Gear-shaped specimen.

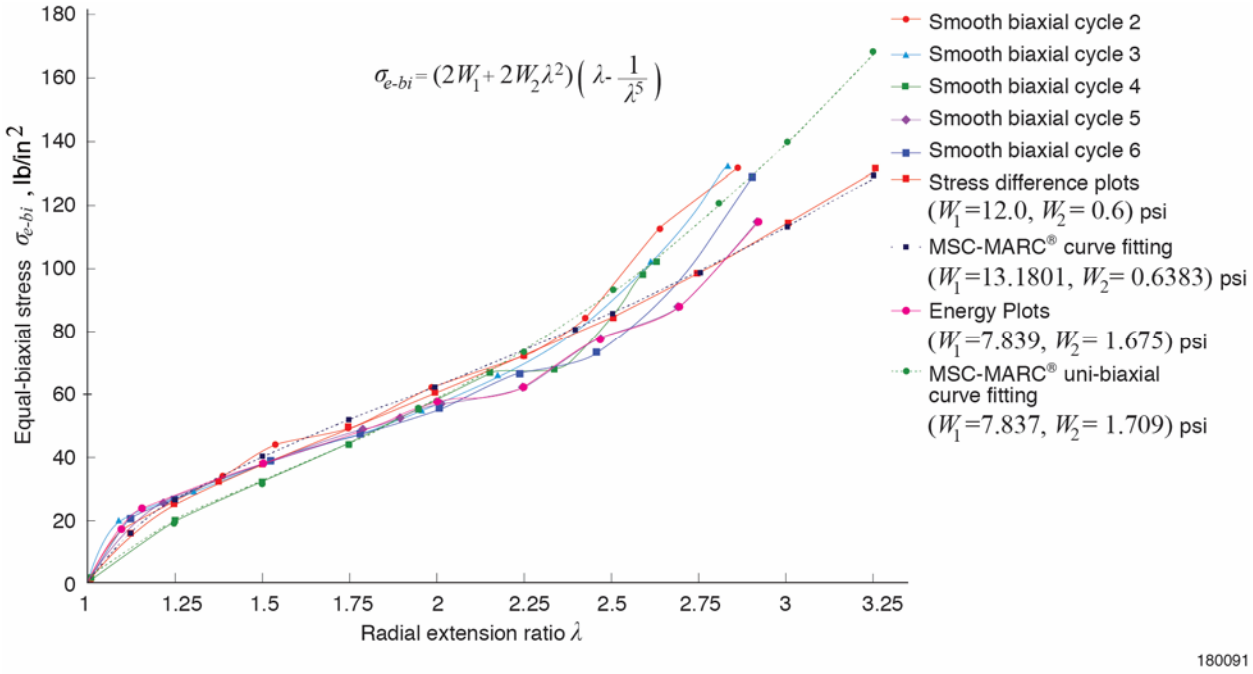

Figure 29(b). Smooth specimen.

Figure 29. Comparisons of theoretical and experimental equal-biaxial stress-stretch curves for silicone rubber.

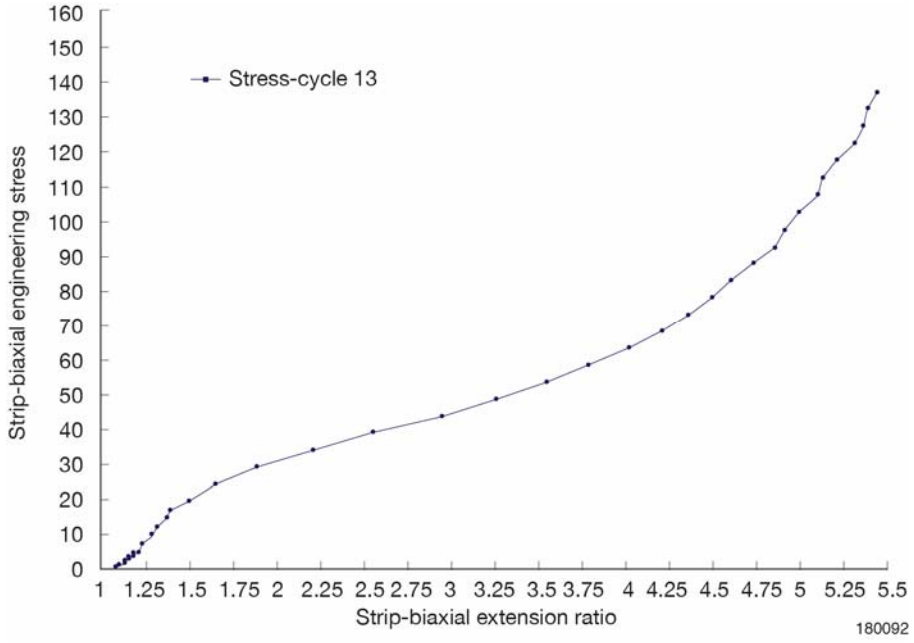

Figure 30. Strip-biaxial stress-stretch curve (stress-cycle 13) of silicone rubber used for the stress-difference plot to determine associated material constants summation $(W_1 + W_2)$.

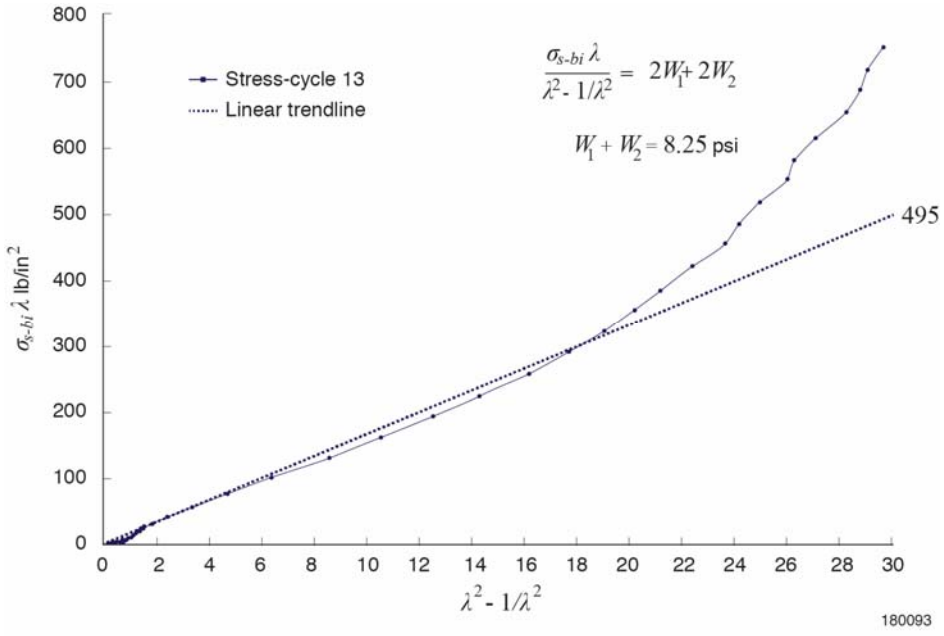

Figure 31. Strip-biaxial stress difference plot [eq. (11)] for determining material constant summation $(W_1 + W_2)$ for silicone rubber using the slope of the linear trendline [$(W_1 + W_2) = 8.25$ lb/in^2].

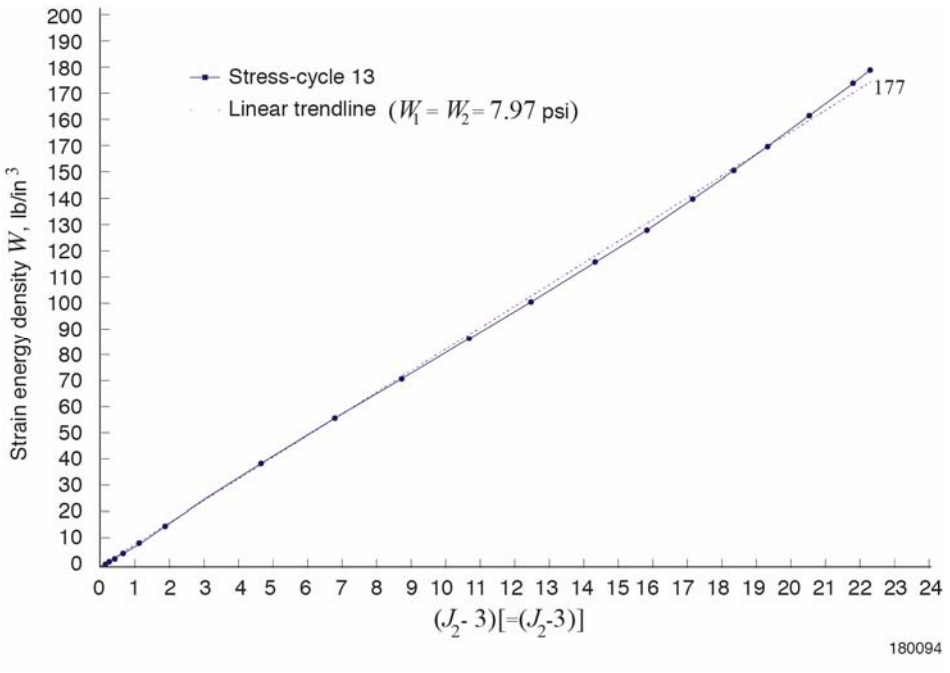

Figure 32. Plots of strip-biaxial strain energy density data of W [eq. (13)] as functions of $(J_1 - 3)[= (J_2 - 3)]$ for determining material constant $W_1 (= W_2)$ for silicone rubber.

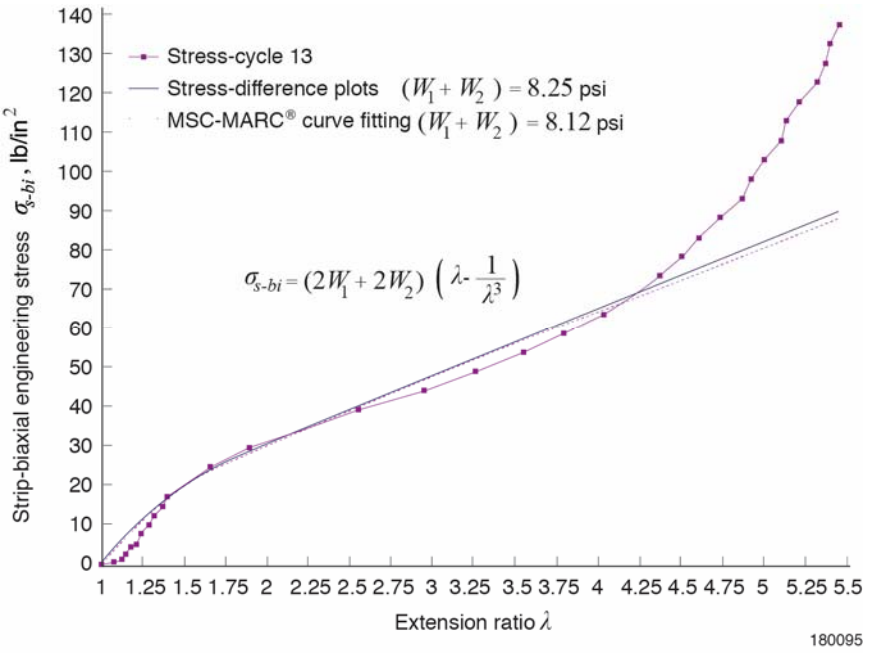

Figure 33. Comparisons of theoretical and experimental strip-biaxial stress-stretch curves for silicone rubber: stress-difference plot $(W_1 + W_2) = 8.25$ lb/in^2 and MSC curve-fitting $(W_1 + W_2) = 8.12$ lb/in^2.

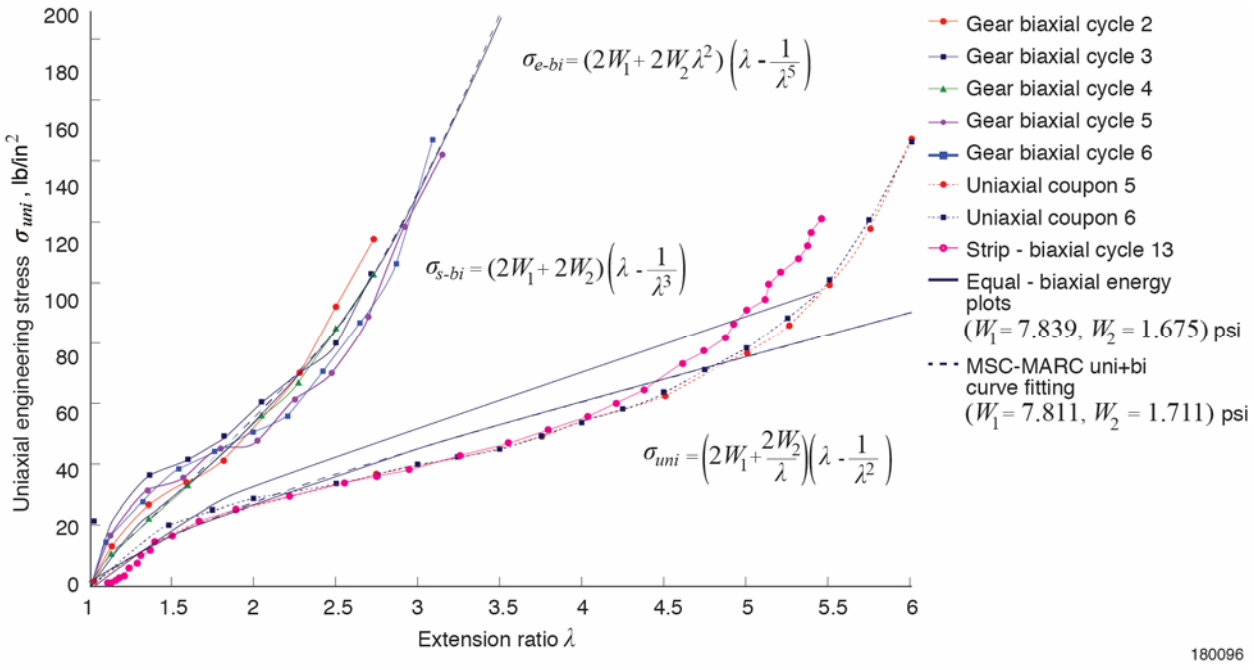

Figure 34(a). Gear-shaped specimen.

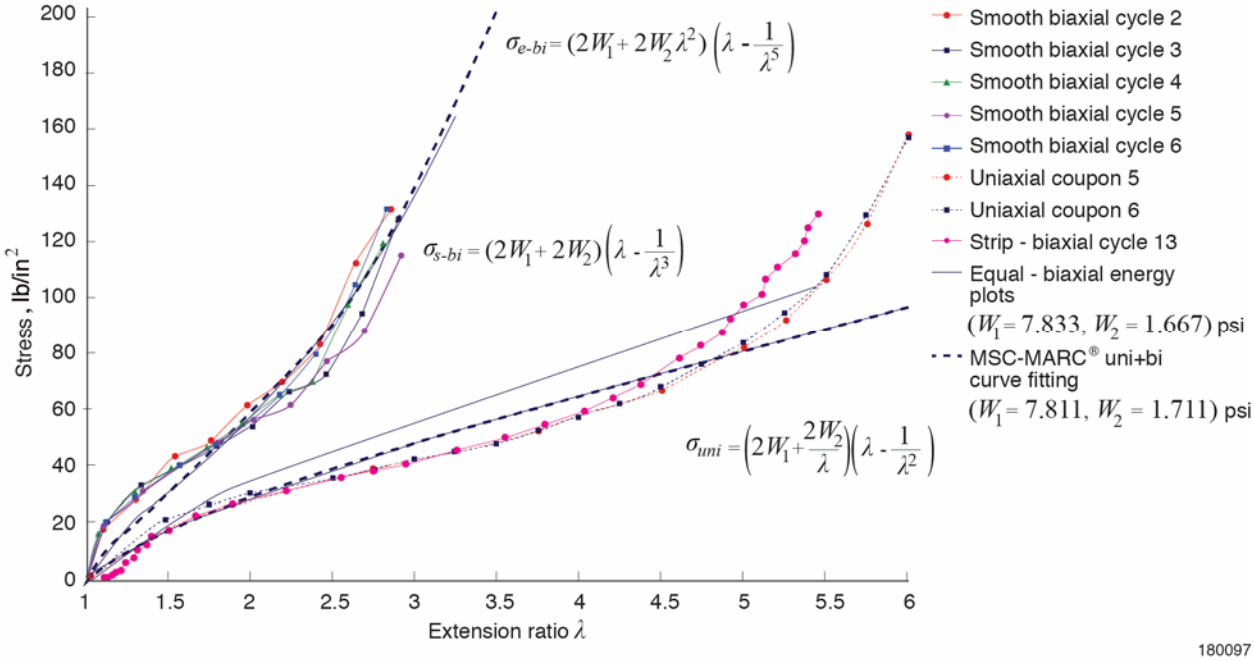

Figure 34(b). Smooth specimen.

Figure 34. Comparisons of theoretical and experimental uniaxial, equal-biaxial, and strip-biaxial stress-stretch curves for the silicone rubber; theoretical curves based on (W_1=7.839, W_2=1.675) lb/in^2 (equal-biaxial energy plots) and based on (W_1=7.811, W_2=1.711) lb/in^2 (MSC-MARC® combined curve fitting).

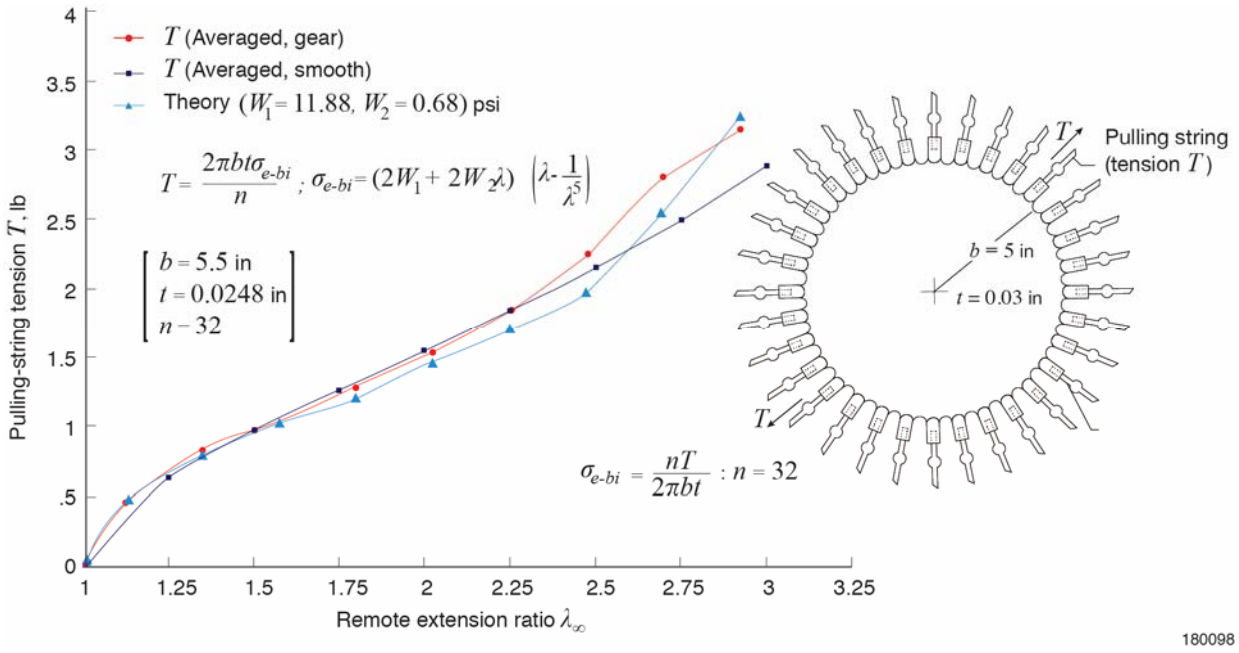

Figure 35. Comparison of measured and theoretically calculated pulling-string tensile forces T required to pull a circular specimen of silicone rubber to the desired radial extension ratio λ; the theoretical calculations based on equal-biaxial material constants ($W_1 = 11.88$. $W_2 = 0.68$) lb/in^2 in the post-stress-cycled dimensions: $b \approx 5.5$ in., $t \approx 0.0248$ in.

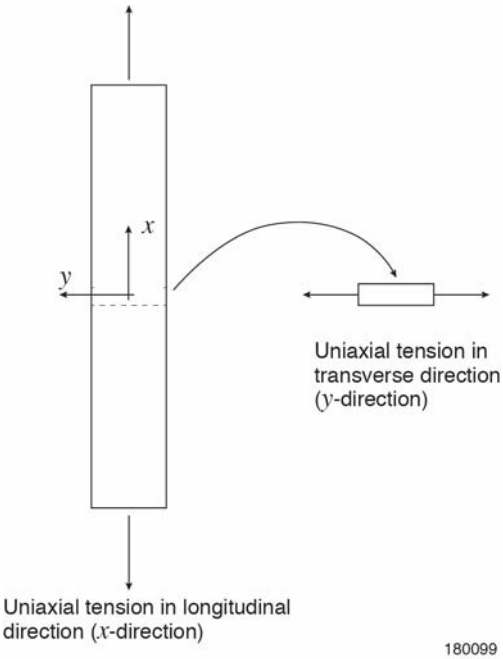

Figure 36. Transverse uniaxial tensile test specimen cut off from a longitudinally tested silicone rubber specimen for exploring transverse uniaxial stress-stretch behavior.

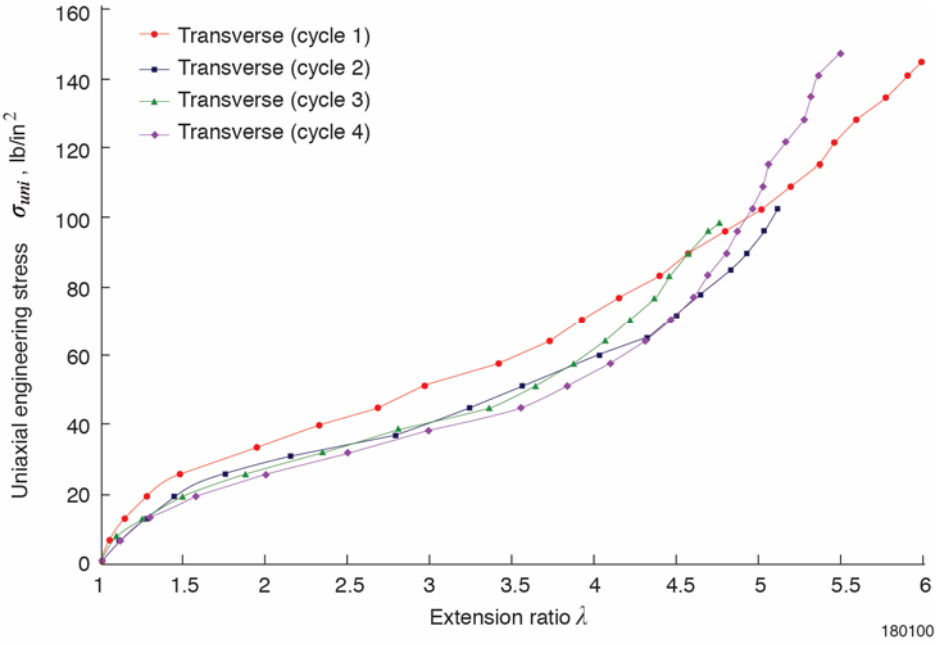

Figure 37. Uniaxial stress-stretch curves obtained from a transverse specimen cut from a longitudinally pre-stretched silicone rubber specimen.

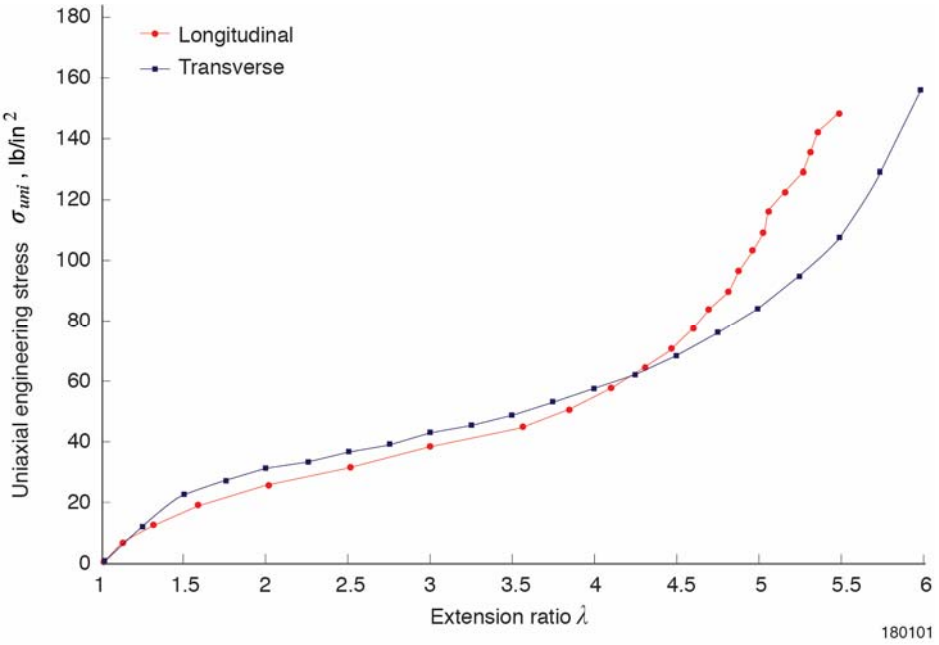

Figure 38. Comparison of longitudinal and transverse uniaxial stress-stretch curves for silicon rubber, showing a marked property difference at high extensions.

Appendix A
Theoretical Pulling String Tension

Using *n* numbers of pulling-string tensile force (*T* lb per pulling string) for radially puling the circular specimen to a desired radial (=tangential) extension ratio λ, the induced equal-biaxial true (Cauchy) stress $\bar{\sigma}_{e-bi}$ referred to the deformed body (deformed radius λb, deformed thickness $\lambda_{th} t$) and the equal-biaxial engineering (Biot) stress σ_{e-bi} referred to the undeformed body (undeformed radius *b*, and undeformed thickness *t*) can be related to the pulling-string tension *T* for incompressible material $(J_3 = \lambda^2 \lambda_{th} = 1)$ as equation (A1):

$$\underbrace{\bar{\sigma}_{e-bi}}_{\text{Equal-biaxial true stress}} = \frac{nT}{\underbrace{2\pi(\lambda b)(\lambda_{th} t)}_{\text{Deformed circuferencial area}}} = \frac{nT\lambda}{2\pi bt \underbrace{(\lambda^2 \lambda_{th})}_{=J_3=1}} = \underbrace{\frac{nT}{2\pi bt}}_{\sigma_{e-bi}} \lambda = \underbrace{\sigma_{e-bi}}_{\text{Equal-biaxial engineering tress}} \lambda \quad ; \quad J_3 = \lambda^2 \lambda_{th} = 1 \tag{A1}$$

In equation (A-1), the equal-biaxial engineering stress σ_{e-bi} is defined as equation (A2):

$$\sigma_{e-bi} = \frac{nT}{2\pi bt} \tag{A2}$$

In equation (A2), σ_{e-bi} can be calculated from the equal-biaxial constitutive equation (7), which is rewritten as equation (A3):

$$\sigma_{e-bi} = \left(2W_1 + 2W_2 \lambda^2\right)\left(\lambda - \frac{1}{\lambda^5}\right) \tag{A3}$$

In view of equations (A2) and (A3), the theoretical tensile force *T* in each pulling string can be expressed as equation (A4):

$$T = \left(\frac{2\pi bt}{n}\right)\left(2W_1 + 2W_2 \lambda^2\right)\left(\lambda - \frac{1}{\lambda^5}\right) \tag{A4}$$

For given material constants $\{W_1, W_2\}$, equation (A4) can be used to estimate the theoretical pulling-string tension *T* for selecting proper pulling-string tension meter.

Appendix B
Lessons Learned from Elastomer Testing

Various lessons learned during the current elastomer testing are listed below:

1) The typical dog-bone shaped coupons do not work well for elastomer testing:
   a) The "weak" area of the coupon is very small which makes it difficult to collect data with the Digital Image Correlation (DIC) system with the lenses we currently have.
   b) When we scaled up to a large enough coupon to take DIC data we lost our ability to reach higher stretch ratios.
   c) The elastomer dog bone coupon stretches throughout the entire coupon (at different rates) eliminating the ability to isolate the "weak" area.

   Solution: In order to overcome these problems we changed the shape of the coupon to a constant one-inch wide. This change helped with the DIC system as we now had more surface area to acquire data from; we could also create this coupon in any length we desired eliminating any problems with the size of our test rig, and eliminating the problems we had with the specimen stretching unevenly.

2) Difficulties with collecting photogrammetry data:
   a) All of our normal methods for applying the speckle pattern required to collect DIC data were useless on the elastomer material, and all of our previous methods involved different ways to apply paint to a specimen. In this case the paint did not stick to the elastomer well, and most of the paint that did stick fell off shortly after we started to stretch the coupon.

   Solution: After experimenting with several different marking materials, we determined that black permanent markers worked best as it stayed on the coupon for at least five or more cycles.

   b) Once we started using this method we discovered another problem; the permanent ink would become more translucent as it was stretched so that we were not able to collect data over about extension ratio $\lambda = 3$.

   Solution: We eventually discovered that if we stretched the coupon to about $\lambda = 3$, and then applied the speckle pattern with the permanent marker that the pattern stayed recognizable to the DIC system to over extension ratio $\lambda = 6$.

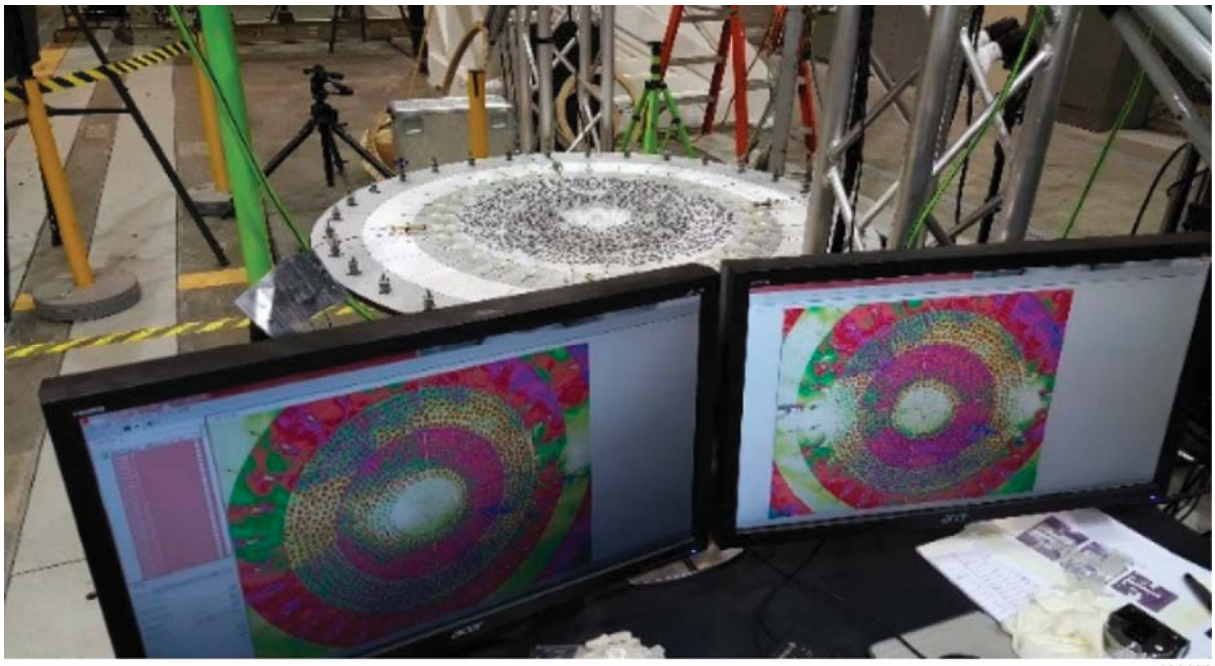

Figure B1. Radially stretched circular biaxial test specimen.

3) Problems with clamps gripping the material to full load:
    a) We tried several different clamping methods to hold the elastomer specimen into the uniaxial test rig. We tried clamps we had, we tried clamps we made and we also purchased a set of self-tightening scissor grip clamps that were designed for the clamping elastomer. In each case the specimen slipped out of the clamp under load, as the elastomer got thinner the grips failed to hold.
    b) One of the methods we tried was to clamp the clamps with vise grips. This clamping method helped but it also increased the incidence of the clamps damaging the specimen and if the elastomer had even the slightest nick it failed very quickly starting at the location of the nick.

Solution: The specimen again had to be modified, but this time not having to rely on the grip strength of the clamps.

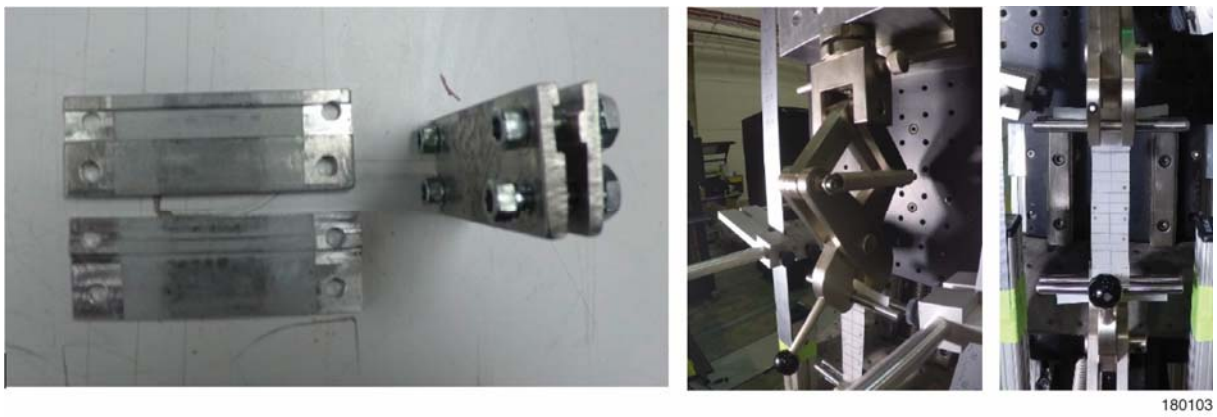

Figure B2. Different types of clamps.

4) Finding the right adhesive and materials to bond to the elastomer:
    a) We tried several different adhesives to bond the elastomer in preparation for building the bi-axial coupons. We tried cyanoacrylate adhesive, epoxy, and clear silicone.
    b) We tried many different materials and methods to bond the material to the elastomer in order to create a link for the bi-axial coupons to be connected into the bi-axial test rig.

Solution: The Dow Corning 3145 clear silicone outperformed the other adhesives by a wide margin, and a wide flat cloth shoestring type material double bonded to both sides of the coupon with an extra piece of elastomer bonded over the “shoestring” allowed for the highest loads before failure of the bond.

Figure B3. Examples of the “shoestring” bonding method.

5) Finding data with digital camera:

As testing went on it was decided that using the DIC system was too time consuming so the data collection method was changed to using digital cameras to take video during the tests and then counting pixels using a software program.

Solution: Ultimately using the digital cameras may have cost more time due to the length of time it took to record the pixel count frame by frame.

6) Designing and building the circular table for biaxial testing:

The parameters given were to design a test rig that would evenly load a 10-in. diameter circular coupon to at least $\lambda = 3$ while constantly measuring the load and extension ratio λ, using a very small budget.

Solution: Many ideas were heard and considered from a large number of consultants. We ultimately decided on a five-foot diameter table with low cost automotive tool type ratcheting mechanisms with pulleys and small cables. Winding the cables around the pulleys using the ratcheting mechanism one at a time incrementally worked well to stretch the coupon evenly to over $\lambda = 3.5$, but a few of the inexpensive ratchets failed and had to be replaced. We did not have any load cells that could meet the size and function requirements of the setup so we acquired a small 4-mini load cell data acquisition system and some digital fish scales in order to acquire the loads and to verify even load distribution.

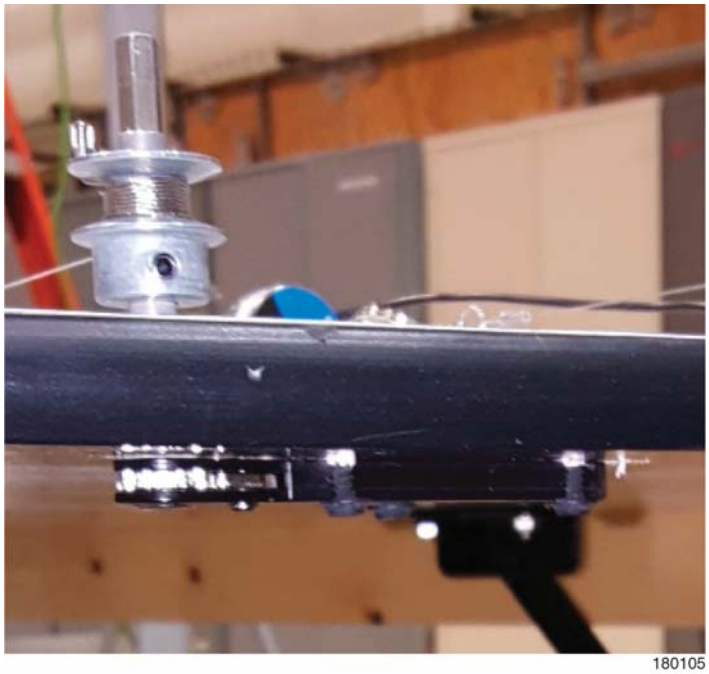

Figure B4. Miniature manual pulley.

Figure B5. Four mini loads cells (eight larger load cells were not needed because of inaccuracy).

References

1. Ko, William L., and Shun-Fat Lung, "Non-Classical Stress Concentration Behavior in a Radially Stretched Hyperelastic Sheet Containing a Circular Hole," NASA/TM-2017-219527, August 2017.

2. Blatz, Paul J., and William L. Ko, "Application of Finite Elastic Theory to the Deformation of Rubbery Materials," *Transactions of the Society of Rheology*, Vol. 6, pp. 223-251, 1962.

3. Ko, William L., "Application of Finite Elastic Theory to the Behavior of Rubber-Like Materials," Ph.D. Dissertation, California Institute of Technology, Pasadena, California, June 1963.

4. Ko, W. L., and P. J. Blatz, "Application of Finite-Anisotropic Elasticity to the Behavior of Natural Rubbers," GALCIT SM 63-39, California Institute of Technology, August 1963.

5. *MSC. NASTRAN 2012 Quick Reference Guide*, The MacNeal Schwendler Corporation, Newport Beach, California, 2012.

6. Ko, W. L., and P. J. Blatz, "Application of Finite Viscoelastic Theory to the Deformation of Rubber-like Materials–Uniaxial Stress Relaxation Data," GALCIT SM 64-4, California Institute of Technology, January 1964.